

VI. CONCLUSION

The measurement method of the optical gain allowed us to distinguish three processes able to provide gain in CdS. The best understood one is due to the annihilation of a free exciton with the emission of an optical phonon and the two other processes are related to interactions between excitons and electrons. The transitions related to bound excitons do not occur in our experiments since the results obtained do not depend on the existence of the I_1 line. In spite of the approximations used in the theoretical treatment and the limitations of the experimental interpretation, we think that we have clearly identified the processes responsible for the laser effect in intrinsic CdS. In addition, we want to point

out that the results obtained by some authors^{20,21} seem to show that the extrinsic process is more efficient than the intrinsic ones to obtain amplification at low injection level.

ACKNOWLEDGMENTS

The authors wish to acknowledge stimulating discussions with Professor Nozières and Professor Hulin, and to thank the Société BARAT for providing them with the CdS samples.

²⁰ C. E. Hurwitz, *Appl. Phys. Letters* **9**, 420 (1966).

²¹ C. W. Litton and D. C. Reynolds, in *Proceedings of the International Conference of II-VI Semiconducting Compounds, Providence, 1967*, edited by D. G. Thomas (W. A. Benjamin, Inc., New York, 1968), p. 694.

Backward Stimulated Raman Scattering*

M. MAIER AND W. KAISER

Physik-Department der Technischen Hochschule, Munich, Germany

AND

J. A. GIORDMAINE

Bell Telephone Laboratories, Murray Hill, New Jersey 07974

(Received 26 August 1968)

This paper describes in detail the initiation and growth of backward-traveling stimulated Raman-Stokes pulses. The radiation-transfer equations for the pulse development are derived, and a general analytic solution is given in the rate-equation approximation. Special solutions are given for a variety of pulse-initiation conditions. It is shown that in the presence of residual linear absorption, a steady-state Stokes pulse is expected, and its characteristics are described. Extensive experimental observations in CS₂ of the properties of the backward pulse and the forward emission are reported, including measurements of the pulse energy as a function of position in the cell, the pulse duration as measured by the intensity-auto-correlation technique, and the time sequence of the emission of the forward and backward pulses. Various experimental results indicate the dominant role played by self-focusing in the initiation of the backward pulse and the role of competing processes. The growth of the pulse energy is found to be consistent with the theory; a minimum pulse duration of 30 psec and a peak pulse power 20 times the instantaneous laser pump power are reported, indicating substantial depletion of the incident laser pump light.

I. INTRODUCTION

SINCE the first observations of stimulated Raman scattering,^{1,2} backward stimulated Stokes emission and the backward/forward intensity ratio r have remained relatively poorly understood. The theory of stimulated Raman scattering³⁻⁶ shows that under

steady-state conditions in the absence of feedback, r should be unity, irrespective of the degree of saturation of the stimulating pump light. Measurements in liquids such as CS₂^{7,8} and benzene⁹ generally show r in the range 0 to 0.5. Furthermore, the time dependence of the backward emission has been shown in deuterium¹⁰ and H₂ gas¹¹ to have complex transient behavior on a nanosecond time scale quite different than the forward behavior.

* Results included in the present paper were presented in part by M. Maier, W. Kaiser, M. Stanka, and J. A. Giordmaine at the International Summer School of Physics "Enrico Fermi," Varenna 1967 (to be published).

¹ E. J. Woodbury and W. K. Ng, *Proc. IRE* **50**, 2347 (1962).

² G. Eckhardt, R. W. Hellwarth, F. J. McClung, S. E. Schwarz, D. Weiner, and E. J. Woodbury, *Phys. Rev. Letters* **9**, 455 (1962).

³ R. W. Hellwarth, *Phys. Rev.* **130**, 1850 (1963).

⁴ E. Garmire, E. Pandarese, and C. H. Townes, *Phys. Rev. Letters* **11**, 160 (1963).

⁵ Y. R. Shen and N. Bloembergen, *Phys. Rev.* **137**, 1787 (1965).

⁶ V. T. Platonenko and R. V. Khokhlov, *Zh. Eksperim. i Teor. Fiz.* **46**, 560 (1964) [English transl.: *Soviet Phys.—JETP* **19**, 378 (1964)].

⁷ B. P. Stoicheff, *Phys. Letters* **7**, 186 (1963).

⁸ G. Bret and G. Mayer, in *Physics of Quantum Electronics*, edited by P. L. Kelley, B. Lax, and P. E. Tannenwald (McGraw-Hill Book Co., New York, 1966).

⁹ P. D. Maker and R. W. Terhune, *Phys. Rev.* **137**, A801 (1965).

¹⁰ R. W. Minck, E. E. Hagenlocker, and W. G. Rado, *Phys. Rev. Letters* **17**, 229 (1966); *J. Appl. Phys.* **38**, 2254 (1967).

¹¹ W. H. Culver, J. T. A. Vanderslice, and V. W. T. Townsend, *Appl. Phys. Letters* **12**, 189 (1968).

Several factors appear to contribute to the anomalous backward/forward ratio. First, a difference in the cross section for forward and backward Raman scattering as small as 10^{-2} could account for some of the observed results, since the gain depends exponentially on the cross section.¹² Second, some of the observations have been made with multimode laser excitation, in which traveling regions of high gain favor forward emission.^{13,14} Third, stimulated Raman emission is usually observed under self-focusing conditions,¹⁵ and indeed in liquids such as CS_2 and benzene having high Kerr constants it is initiated by self-focusing.^{16,17} It has been shown that instabilities in self-focusing give rise to local regions of high gain having a lifetime less than 1 nsec.¹⁸ Recurrence of this effect along the beam represents a traveling high-gain region, again favoring forward emission. The importance of self-focusing is clearly shown in experiments on CS_2 -acetone solutions in which stimulated acetone Raman scattering can be observed with and without self-focusing.¹⁹ In the absence of self-focusing a ratio $r = 1$ was believed to have been observed.

In a recent letter,²⁰ the present authors called attention to a fundamental difference in the behavior of backward and forward stimulated scattering. A forward-traveling Stokes pulse has access only to the pump energy stored in the traveling volume element occupied by the pulse, since the Stokes and pump light travel at approximately the same velocity. As a result pump saturation limits the pulse intensity to a value less than the initial pump intensity. On the other hand, a backward-traveling pulse continuously encounters undepleted pump light, and the leading edge can be amplified to a value far in excess of the pump intensity. At high intensities the pulse may in fact sweep out the incoming pump beam leaving the cell momentarily without pump light. Accompanying the high amplification of the pulse is a strong steepening and sharpening of the pulse as the pump beam becomes converted in a decreasing distance near the leading edge. It has been found that transient pulses initiated by self-focusing in CS_2 can be amplified to 20 times the pump intensity

¹² N. Bloembergen and Y. R. Shen, Phys. Rev. Letters **12**, 504 (1964).

¹³ N. Bloembergen and Y. R. Shen, Phys. Rev. Letters **13**, 720 (1964).

¹⁴ W. G. Wagner, S. Yatsiv, and R. W. Hellwarth, in *Physics of Quantum Electronics*, edited by P. L. Kelley, B. Lax, and P. E. Tannenwald (McGraw-Hill Book Co., New York, 1966).

¹⁵ G. Hauchecorne and G. Mayer, Compt. Rend. **261**, 4014 (1965); Y. R. Shen and Y. J. Shaham, Phys. Rev. Letters **15**, 1008 (1965); P. Lallemand and N. Bloembergen, *ibid.* **15**, 1010 (1965).

¹⁶ C. C. Wang, Phys. Rev. Letters **16**, 344 (1966).

¹⁷ M. Maier and W. Kaiser, Phys. Letters **21**, 529 (1966).

¹⁸ R. Y. Chiao, M. A. Johnson, S. Krinsky, H. A. Smith, C. H. Townes, and E. Garmire, IEEE J. Quantum Electron. **2**, 467 (1966); D. H. Close, D. R. Giuliano, R. W. Hellwarth, L. D. Hess, F. J. McClung, and W. G. Wagner, *ibid.* **2**, 553 (1966); R. G. Brewer, J. R. Lifshitz, E. Garmire, R. Y. Chiao, and C. H. Townes, Phys. Rev. **166**, 326 (1968).

¹⁹ G. Bret and M. Denariez, Appl. Phys. Letters **8**, 151 (1966).

²⁰ M. Maier, W. Kaiser, and J. A. Giordmaine, Phys. Rev. Letters **17**, 1275 (1966).

with a pulse duration of approximately 30 psec. This process plays a key role in the transient behavior of the stimulated Raman and Brillouin effects particularly in the presence of self-focusing. The process in addition provides a source of 10^{-10} - to 10^{-11} -sec light pulses of possible use in other optical experiments. Further discussion of this process is given in Refs. 11, 21, and 22.

The present paper describes in detail the initiation and growth of backward-traveling Stokes pulses and presents further experimental evidence which clarifies the initiation mechanism. Section II contains the derivation of the radiation transfer or rate equations. In Secs. III and IV the analytical solution of the radiation transfer equations is given and discussed for various initial conditions. In Sec. V it is shown that the backward Raman pulse approaches a limiting steady-state pulse shape. The width and intensity of the steady-state pulse are calculated. The experimental apparatus and the experimental results are described in Secs. VI and VII, respectively, followed by discussion in Sec. VIII. Appendix A discusses theoretical details of the pulse formation for special initial conditions, while in Appendix B the relation between the spontaneous Raman scattering data and the gain factor for stimulated Raman scattering is derived.

II. RADIATION TRANSFER EQUATIONS

We adopt as a model of liquid CS_2 an ensemble of noninteracting, axially symmetric, randomly oriented molecules having the strongest Raman-active vibration along the axis of symmetry. Other vibrations may be ignored. Let $\alpha_{xx'}$, $\alpha_{zz'}$ be the nonvanishing molecular susceptibilities in a molecular fixed coordinate system $x'y'z'$, in which z' is the symmetry axis. The change in α_{ij}' with a displacement q' of the normal vibrational coordinate is given by

$$\alpha_{xx'} = \alpha_{xx'}(0) + \frac{\partial \alpha'_{xx}}{\partial q} q' \quad \text{and} \quad \alpha_{zz'} = \alpha_{zz'}(0) + \frac{\partial \alpha'_{zz}}{\partial q} q'.$$

When we average over the random orientations of the ensemble we obtain an effective molecular polarizability

$$\alpha(0) + \frac{\partial \alpha}{\partial q} q' = \left[\frac{2}{3} \alpha_{xx'}(0) + \frac{1}{3} \alpha_{zz'}(0) \right] + \left[\frac{2}{3} \frac{\partial \alpha_{xx'}}{\partial q} + \frac{1}{3} \frac{\partial \alpha_{zz'}}{\partial q} \right] q'. \quad (2.1)$$

The CS_2 molecule may be represented for our purposes as a two-level system consisting of the ground (000) and first excited (100) vibrational states, with frequency separation $\bar{\nu} = \omega/2\pi c = 656 \text{ cm}^{-1}$. The full width at half-

²¹ A. J. Glass, IEEE J. Quantum Electron. **3**, 516 (1967).

²² S. A. Akhmanov, A. S. Chirkin, K. N. Drapovich, A. I. Kovrigin, R. V. Khokhlov, and A. O. Sukhorkov (to be published).

maximum intensity of the (100) ← (000) transition in liquid CS₂ is $\Delta\bar{\nu} = \Delta\omega/2\pi c = 0.50 \text{ cm}^{-1}$.²³ Anharmonicity gives rise to a difference of 2.7 cm⁻¹ between the (100) ← (000) and (200) ← (100) transitions,²⁴ and justifies the two-level approximation.

The Hamiltonian of a two-level system having the polarizability (2.1), in the absence of a permanent dipole moment, is given in the electric dipole approximation by (2.2)

$$\mathcal{H} = \mathcal{H}^0 - \frac{1}{2} q' E^2, \quad (2.2)$$

where q' is the operator representing the oscillator displacement and E is the applied electric field. \mathcal{H}^0 represents the total Hamiltonian of the molecule in the absence of field, and the two levels are eigenstates of \mathcal{H}^0 . Let a_0 and a_1 represent the amplitudes of the states (000) and (100) in the Schrodinger representation. We define

$$\Delta = a_0 a_0^* - a_1 a_1^*, \quad (2.3)$$

the difference in probability of finding the molecule in the ground and excited state. Let N be the molecular density, so that $N\Delta$ represents the population difference density between ground and excited states. Let

$$q_{av} = \langle q' \rangle, \quad (2.4)$$

the expectation value of the displacement operator q' .

It has recently been shown by two of the present authors²⁵ using the methods of Ref. 26 that the equations of motion of Δ and q_{av} , which are ordinary numbers, are given by

$$\frac{\partial^2 q_{av}}{\partial t^2} + \Gamma \frac{\partial q_{av}}{\partial t} + \omega_0^2 q_{av} = \frac{1}{2m} \frac{\partial \alpha}{\partial q} E^2 \Delta, \quad (2.5)$$

$$P = N \frac{\partial \alpha}{\partial q} q_{av} E, \quad (2.6)$$

$$\frac{\partial \Delta}{\partial t} = -\frac{1}{\hbar \omega_0} \left(\frac{\partial \alpha}{\partial q} \right) E^2 \frac{\partial q_{av}}{\partial t} + \Gamma'(1 - \Delta), \quad (2.7)$$

$$\frac{\partial^2 E}{\partial z^2} - \frac{1}{c^2} \frac{\partial^2 D}{\partial t^2} = \frac{4\pi}{c^2} \frac{\partial^2 P}{\partial t^2}, \quad (2.8)$$

where m is the effective mass associated with the q vibration. In Eq. (2.5) the damping constant $\Gamma = \Delta\omega$ has been introduced phenomenologically and corresponds to $1/T_2$ in the Bloch equations. The damping constant Γ' corresponding to $1/T_1$ in the Bloch equations is the

²³ W. R. L. Clements and B. P. Stoicheff, Appl. Phys. Letters 12, 246 (1968).

²⁴ J. Brandmüller and H. Moser, *Einführung in die Raman-spektroskopie* (Dr. Dietrich Steinkopff Verlag, Darmstadt, Germany, 1962).

²⁵ J. A. Giordmaine and W. Kaiser, Phys. Rev. 144, 676 (1966). The expressions for \mathcal{H}' and F in Eqs. (2) and (3) should be multiplied by $\frac{1}{2}$. Equation (9) should read $\hbar\omega_0(d\delta/dt) = -2F(dq/dt)$.

²⁶ E. T. Jaynes and F. W. Cummings, Proc. IEEE 51, 89 (1963).

inverse lifetime of the excited vibrational state. In Eq. (2.7) the equilibrium value of Δ has been assumed 1, i.e., $\hbar\omega_0 \gg kT$. The optical electric field E , displacement vector D , and polarization vector P are assumed to be plane waves linearly polarized along the x axis, and to propagate in the $\pm z$ directions.

The electric field E is assumed to have the form

$$E = E_S \cos(\omega_S t - k_S z) + E_L \cos(\omega_L t + k_L z), \quad (2.9)$$

where the real amplitudes E_S and E_L of the Stokes and pump fields are slowly varying functions of z and t , with $|\partial E_{S,L}/\partial t| \ll |E_{S,L}| \omega_{S,L}$; $|\partial E_{S,L}/\partial z| \ll k_{S,L} |E_{S,L}|$. We consider here only the resonant case

$$\omega_L - \omega_S = \omega_0. \quad (2.10)$$

The expectation value q_{av} of the molecular displacement has the form

$$q_{av} = q \sin(\omega_0 t + k_0 z + \varphi_0), \quad (2.11)$$

with q slowly varying in the same sense as E_S and E_L and $k_0 = k_L + k_S$. We discuss solutions in the approximation that the phase $\varphi_0 = 0$. We provide for finite attenuation constants γ_S and γ_L at the Stokes and pump frequencies, arising from scattering or other linear losses. Finally we allow Δ to be a slowly varying function of z and t . Substitution of (2.9)–(2.11) into (2.5)–(2.8) leads to the coupled amplitude equations

$$\frac{\partial q}{\partial t} + \frac{1}{2} \Gamma q = -\frac{1}{4m\omega_0} \frac{\partial \alpha}{\partial q} E_L E_S \Delta, \quad (2.12)$$

$$\frac{\partial \Delta}{\partial t} = \frac{1}{2\hbar} \frac{\partial \alpha}{\partial q} E_L E_S q + \Gamma'(1 - \Delta), \quad (2.13)$$

$$\frac{\partial E_S}{\partial z} + \frac{n_S}{c} \frac{\partial E_S}{\partial t} + \frac{1}{2} \gamma_S E_S = -\frac{\pi N \omega_S}{n_{SC}} \frac{\partial \alpha}{\partial q} E_L q, \quad (2.14)$$

$$\frac{\partial E_L}{\partial z} - \frac{n_L}{c} \frac{\partial E_L}{\partial t} - \frac{1}{2} \gamma_L E_L = -\frac{\pi N \omega_L}{n_{LC}} \frac{\partial \alpha}{\partial q} E_S q. \quad (2.15)$$

Equations (2.12) and (2.13) contain the same information as the equations of motion of the elements of the density matrix for the molecules.

In the rate-equation approximation we set

$$\partial q / \partial t \ll \frac{1}{2} \Gamma q; \quad (2.16)$$

i.e., the vibrations are heavily damped. The photon flux cm⁻² sec⁻¹ $N_{L,S}$ is given in terms of $E_{L,S}$ by

$$N_{L,S} = \frac{cn}{8\pi\hbar\omega_{L,S}} E_{L,S}^2, \quad (2.17)$$

where $n_L \approx n_S \equiv n$. Substitution of (2.16) and (2.17) into (2.12)–(2.15) yields the radiation transfer equations

$$\frac{\partial N_S}{\partial z} + \frac{n}{c} \frac{\partial N_S}{\partial t} + \gamma_S N_S = \frac{\sigma n}{c} N_S N_L \Delta, \quad (2.18)$$

$$\frac{\partial N_L}{\partial z} - \frac{n}{c} \frac{\partial N_L}{\partial t} - \gamma_L N_L = -\frac{\sigma n}{c} N_S N_L \Delta, \quad (2.19)$$

$$\frac{\partial \Delta}{\partial t} = -\frac{2\sigma n}{cN} N_S N_L \Delta + \Gamma'(1-\Delta), \quad (2.20)$$

where σ , which represents the cross section for the interaction of a pump photon with a Stokes photon, is given by

$$\sigma = \frac{8\pi^2 \hbar \omega_L \omega_S N (\partial \alpha / \partial q)^2}{cm \Gamma \omega_0 n^3}. \quad (2.21)$$

The cross section σ is related to the power gain factor g for stimulated Raman scattering (3.3) by

$$\sigma = g c \hbar \omega_L / n. \quad (2.22)$$

In the experiments to be described below the rate constant $2\sigma N_S N_L n / c N$ for the change of population density $N\Delta$ is typically 10^5 sec^{-1} ; therefore, Δ does not depart significantly from unity during the 20-nsec laser pulse. In Sec. III we use the approximation

$$\Delta = 1.$$

III. GENERAL SOLUTION OF THE RADIATION TRANSFER EQUATIONS

We discuss the solution of the radiation transfer Eqs. (2.18)–(2.20) for the one-dimensional geometry of Fig. 1(a). At time $t=0$, a Stokes beam and a pump beam having fluxes N_S and N_L photons $\text{cm}^{-2} \text{ sec}^{-1}$ are incident on the Raman cell.²⁷

The following approximations will be made: (1) the linear attenuation of N_S and N_L is ignored, $\gamma_S = \gamma_L = 0$; (2) the molecular vibrational ground-state population is not significantly changed, $\Delta = 1$; (3) the forward Stokes flux in the pump beam direction is ignored; this approximation is appropriate for our experiments, in which an initiation mechanism such as pump beam self-focusing at $z=0$ provides a backward Stokes flux at $z=0$ much more intense than the incident flux of quantum noise at $z=l$ in the forward direction; (4) anti-Stokes and parasitic second- and higher-order Stokes generation are ignored. The latter processes are known to be present (see below) and may determine the limiting pulse width.

The rate equations written in terms of photon densities $\eta_{S,L} = n N_{S,L} / c$ become

$$\frac{\partial \eta_S}{\partial z} + \frac{n}{c} \frac{\partial \eta_S}{\partial t} = \sigma \eta_S \eta_L, \quad (3.1)$$

$$\frac{\partial \eta_L}{\partial z} - \frac{n}{c} \frac{\partial \eta_L}{\partial t} = \sigma \eta_S \eta_L. \quad (3.2)$$

²⁷ The initial conditions shown in Fig. 1(a) are a simplified model of the true experimental initial conditions, which will be discussed in Sec. VIII.

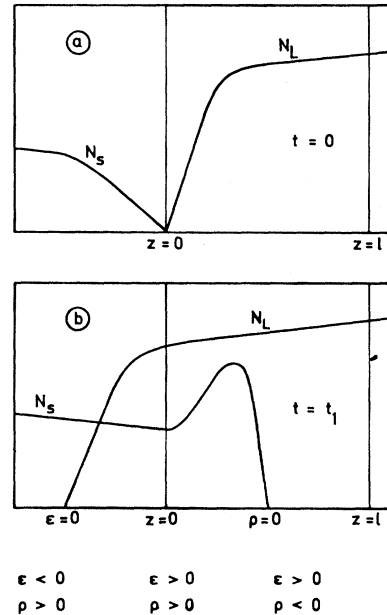


Fig. 1. (a) Initial conditions (schematic) for Stokes and laser photon flux cm^{-2} , N_S and N_L , at time $t=0$. The entrance and exit window of the cell are marked by $z=l$ and $z=0$, respectively. The magnitude of N_S is highly exaggerated compared to N_L . (b) Schematic picture of N_S and N_L at a later time t_1 . $\epsilon=0$ and $\rho=0$ mark the leading edge of the laser and Stokes pulse.

The cross section σ is defined by Eq. (2.21) and its relation to the spontaneous Raman scattering cross section is given in Appendix B. The steady-state gain constant for weak Stokes light in a pump flux η_L is

$$G(\eta_L) \equiv \sigma \eta_L = g I_L, \quad (3.3)$$

where I_L is the laser intensity and g the gain factor for stimulated Raman scattering. The rate equations (3.1) and (3.2) are solved by an extension of the techniques of Refs. 28–33. We introduce the new variables

$$\rho = t - nz/c, \quad (3.4)$$

and

$$\epsilon = t + nz/c, \quad (3.5)$$

and substitute η_L evaluated from (3.1) into (3.2) to obtain the second-order partial differential equation

²⁸ R. Bellman, G. Birnbaum, and W. G. Wagner, *J. Appl. Phys.* **34**, 780 (1963).

²⁹ L. M. Frantz and J. S. Nodvik, *J. Appl. Phys.* **34**, 2346 (1963).

³⁰ J. E. Geusic and H. E. D. Scovil, in *Quantum Electronics*, edited by P. Grivet and N. Bloembergen (Columbia University Press, New York, 1964).

³¹ E. O. Schultz-Du Bois, *Bell System Tech. J.* **43**, 625 (1964).

³² N. G. Basov *et al.*, *Zh. Eksperim. i Teor. Fiz.* **47**, 1595 (1964) [English transl.: *Soviet Phys.—JETP* **20**, 1072 (1965)]; *Opt. i Spektroskopiya* **18**, 1042 (1965) [English transl.: *Opt. Spectry. (USSR)* **18**, 586 (1965)]; *Zh. Eksperim. i Teor. Fiz.* **50**, 23 (1966) [English transl.: *Soviet Phys.—JETP* **23**, 16 (1966)].

³³ R. V. Ambartsumyan *et al.*, *Zh. Eksperim. i Teor. Fiz. Pis'ma v Redaktsiyu* **4**, 19 (1966) [English transl.: *JETP Letters* **4**, 12 (1966)].

(3.6) for $\eta_S(\rho, \epsilon)$:

$$\frac{\partial}{\partial \rho} \left(\frac{1}{\eta_S} \frac{\partial \eta_S}{\partial \epsilon} \right) = \frac{\sigma c}{2n} \frac{\partial \eta_S}{\partial \epsilon}. \quad (3.6)$$

Rearrangement and interchange of the order of differentiation lead to Eq. (3.7):

$$\frac{\partial}{\partial \epsilon} \left(\frac{\partial \ln \eta_S}{\partial \rho} + \frac{\sigma c}{2n} \eta_S \right) = 0.$$

It follows that

$$\frac{1}{\eta_S} \frac{\partial \eta_S}{\partial \rho} + \frac{\sigma c}{2n} \eta_S = f(\rho)$$

and

$$\frac{\partial}{\partial \rho} \left(\frac{1}{\eta_S} \right) + \frac{1}{\eta_S} f(\rho) = \frac{\sigma c}{2n}. \quad (3.7)$$

The first-order linear differential equation (3.7) has the solution

$$\frac{1}{\eta_S} = \frac{\int (\sigma c / 2n) h'(\rho) d\rho + g(\epsilon)}{h'(\rho)}, \quad (3.8)$$

where $h'(\rho) \equiv \exp[\int f(\rho) d\rho]$. From (3.8) and (3.1) η_S and η_L can be written as

$$\eta_S(\rho, \epsilon) = \frac{h'(\rho)}{(\sigma c / 2n) h(\rho) + g(\epsilon)}, \quad (3.9)$$

$$\eta_L(\rho, \epsilon) = \frac{(-2n / \sigma c) g'(\epsilon)}{(\sigma c / 2n) h(\rho) + g(\epsilon)}, \quad (3.10)$$

where $g'(\epsilon) \equiv \partial g / \partial \epsilon$.

Appropriate boundary conditions are $\eta_L(0, \epsilon)$ and $\eta_S(\rho, 0)$. We assume that $\eta_L(0, \epsilon) = 0$ for $\epsilon < 0$, and $\eta_S(\rho, 0) = 0$ for $\rho < 0$ [Fig. 1(b)]. These boundary conditions fix the pump photon density $\eta_L(0, \epsilon)$ encountered by the leading edge ($\rho = 0$) of the Stokes flux, and the Stokes photon density $\eta_S(\rho, 0)$ seen at the leading edge ($\epsilon = 0$) of the pump flux.

Substitution of the boundary conditions in (3.9) and (3.10) leads to first-order linear differential equations for $g(\epsilon)$ and $h(\rho)$, with solutions

$$g(\epsilon) = g(0) + M [e^{-\sigma c D_L(\epsilon) / 2n} - 1], \quad (3.11)$$

$$h(\rho) = \frac{2n}{\sigma c} [M e^{-\sigma c D_S(\rho) / 2n} - g(0)]. \quad (3.12)$$

In (3.11) and (3.12), M is an integration constant and

$$D_L(\epsilon) = \int_0^\epsilon \eta_L(0, y) dy, \quad (3.13)$$

$$D_S(\rho) = \int_0^\rho \eta_S(y, 0) dy. \quad (3.14)$$

The general solution of (3.1) and (3.2) is

$$\eta_S(\rho, \epsilon) = \frac{\eta_S(\rho, 0) e^{\sigma c D_S(\rho) / 2n}}{e^{\sigma c D_S(\rho) / 2n} + e^{-\sigma c D_L(\epsilon) / 2n} - 1}, \quad (3.15)$$

$$\eta_L(\rho, \epsilon) = \frac{\eta_L(0, \epsilon) e^{-\sigma c D_L(\epsilon) / 2n}}{e^{\sigma c D_S(\rho) / 2n} + e^{-\sigma c D_L(\epsilon) / 2n} - 1}. \quad (3.16)$$

We shall approximate (3.15) and (3.16) by (3.17) and (3.18) since the attenuation of pump light in the initial Stokes beam between 0 and ρ is negligible, i.e., $\sigma c D_S(\rho) / 2n \ll 1$.

$$\eta_S(\rho, \epsilon) = \frac{\eta_S(\rho, 0)}{\sigma c D_S(\rho) / 2n + \exp[-\sigma c D_L(\epsilon) / 2n]}, \quad (3.17)$$

$$\eta_L(\rho, \epsilon) = \frac{\eta_L(0, \epsilon) \exp[-\sigma c D_L(\epsilon) / 2n]}{\sigma c D_S(\rho) / 2n + \exp[-\sigma c D_L(\epsilon) / 2n]}. \quad (3.18)$$

Equations (3.17) and (3.18) give the general solution of the radiation transfer equations for the boundary conditions specified in Fig. 1 and otherwise arbitrary initial conditions. In Sec. IV solutions for special initial conditions will be discussed.

IV. SOLUTIONS FOR PARTICULAR INITIAL CONDITIONS

In the first part of this section the phenomena of pulse formation, pulse steepening, and pulse sharpening will be illustrated for several simplified initial conditions. In the second part initiation by physically more realistic Raman input pulses is investigated. The results of these calculations are compared in Sec. VIII with the experimental results.

The boundary conditions specifying η_S and η_L at $\epsilon = 0$ and $\rho = 0$ are not convenient for discussion of the experiments reported here. Since the source of incident Raman light is in fact localized at $z = 0$, we wish to express the Stokes flux $\eta_S(z = l, t)$ as a function of $\eta_S(z = 0, t)$. The required technique is most easily seen by considering specific examples of time dependence of the initiating Stokes flux $\eta_S(0, t)$.

For all cases the incident pump flux will be considered to have the constant value η_{L0} for $\epsilon = t + nz/c > 0$:

$$\eta_L(0, \epsilon) = \eta_{L0}, \quad D_L(\epsilon) = \eta_{L0} \epsilon, \quad \epsilon > 0 \\ = 0, \quad = 0, \quad \epsilon \leq 0. \quad (4.1)$$

The gain constant for Stokes light near the leading edge of the Stokes pulse is $G(\eta_{L0}) \equiv G_0 = \sigma \eta_{L0}$.

A. Step-Function Initiation

$$\eta_S(z = 0, t) = \eta_{S0}, \quad t > 0 \\ = 0, \quad t \leq 0. \quad (4.2)$$

It will be seen below [Eq. (4.5)] that an accurate approximation to this boundary condition is obtained by substituting for $\eta_S(\rho, 0)$ in (3.17) and (3.18) the func-

tions

$$\eta_S(\rho, 0) = \eta_{S0} e^{-Gc\rho/2n}, \quad \rho > 0$$

$$= 0, \quad \rho \leq 0 \quad (4.3)$$

and

$$D_S(\rho) = \frac{2\eta_{S0}n}{Gc} (1 - e^{-Gc\rho/2n}), \quad \rho > 0$$

$$= 0, \quad \rho \leq 0. \quad (4.4)$$

Equation (4.3) is introduced since there is no amplification of Stokes light outside the liquid cell ($z < 0, \rho > 0$).

From (3.17), (3.18), (4.3), and (4.4) the resulting value of $\eta_S(0, t)$ is

$$\eta_S(0, t) = \frac{\eta_{S0}}{1 + \eta_{S0}/\eta_{L0}(e^{Gct/2n} - 1)}. \quad (4.5)$$

If $\eta_{S0}/\eta_{L0} < 10^{-4}$, $\eta_S(0, t)$ differs from η_{S0} by less than 1% for $Gct/2n < 4$, and demonstrates the validity of approximation (4.3) for small times ($t < 6 \times 10^{-10}$ sec for $G = 0.7 \text{ cm}^{-1}$).

The time dependence $\eta_S(l, t)$ is given by (4.6) in terms of the parameters defined in (4.7) and (4.8):

$$\frac{\eta_S}{\eta_{L0}} = \frac{R}{1 + R(e^y - 1)}, \quad y > 0 \quad (4.6)$$

where

$$R = (\eta_{S0}/\eta_{L0}) e^{Gt} \quad (4.7)$$

and

$$y = \frac{1}{2}G \left(\frac{c}{n} t - l \right) = \frac{Gc}{2n} (t - t_0). \quad (4.8a)$$

The parameter R is the peak Stokes photon density in units of incident pump density; y is the time after arrival of the pulse leading edge at t_0 , in units of $2n/Gc$. The peak pulse intensity occurs at the leading edge of the pulse and grows exponentially with gain constant G measured in cm^{-1} .

In order to compare different initial conditions a reference length l_0 is introduced in the following discussions. For all initial conditions l_0 is defined as the distance for which $\eta_S(\text{max})/\eta_{L0}$ is 10^{-2} . For initial condition A the ratio of the peak pulse intensity to the laser intensity $\eta_S(\text{max})/\eta_{L0}$ is given by R . From the definition of the reference length l_0

$$[\eta_S(\text{max})/\eta_{L0}]_{l_0} = R(l_0) \equiv R_0 = 10^{-2}$$

and from Eq. (4.7) we obtain

$$e^{Gt_0} = \frac{R_0}{\eta_{S0}/\eta_{L0}}. \quad (4.8b)$$

Equation (4.7) can be rewritten in the form

$$R = R_0 e^{G(t-t_0)} = 10^{-2} e^{G(t-t_0)}, \quad (4.9)$$

which has been used to calculate the results shown in

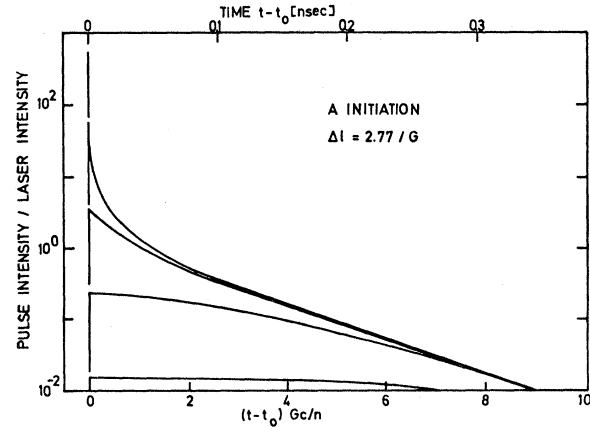


FIG. 2. Calculated normalized Raman pulse intensity as a function of time t for initial condition A (step function). t_0 is the leading edge of the pulse. The curves show the pulse development at length intervals of $\Delta l = 2.77/G$. G is the Raman gain and was determined to be 0.7 cm^{-1} in CS_2 for our experimental system. Lower scale is in dimensionless units; upper scale describes our experimental conditions.

Figs. 5-7. The total number of photons cm^{-2} in the pulse is

$$n_S(l) = \int_{t_0}^{\infty} \eta_S(l, t) dt = \frac{2}{\sigma} \frac{R}{R-1} \ln R \quad (4.10)$$

and the full length at half-maximum intensity

$$\delta = (2/G) \ln(1 + 1/R). \quad (4.11)$$

In the limit $R \gg 1$,

$$n_S \approx 2\eta_{L0}l + (2/\sigma) \ln(\eta_{S0}/\eta_{L0}) = (2/\sigma)G(l-l_0) + (2/\sigma) \ln R_0 \quad (4.12)$$

and

$$\delta \approx 2/(RG). \quad (4.13)$$

This result shows that when the peak Stokes photon density becomes large relative to η_{L0} , the pulse acquires $2\eta_{L0}$ photons per cm of travel, corresponding to complete depletion of the incoming pump beam. The total number of photons per cm^2 can be used to calculate the energy E_S in the pulse with the relation

$$E_S = (n_S \sigma) (\omega_S n F / \omega_L c g) = n_S \hbar \omega_S F.$$

For $R \gg 1$,

$$E_S = 2 \frac{n \omega_S}{c \omega_L} P_L (l-l_0) + 2 \frac{n \omega_S F}{c \omega_L g} \ln R_0. \quad (4.14)$$

P_L is the laser power, F the area of the laser beam, and g the gain factor for stimulated Raman scattering.

Figure 2 shows the pulse time dependence calculated from (4.6) at several equal intervals of l . The characteristic rapid sharpening of the pulse for $\eta_S/\eta_{L0} > 1$ is clearly shown.

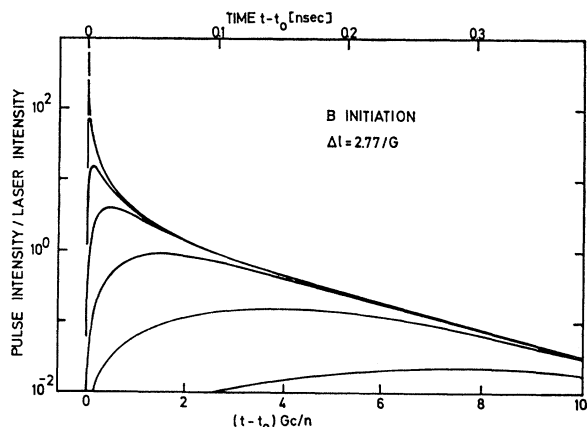


FIG. 3. Calculated normalized Raman pulse intensity as a function of time t for initial condition B (linear ramp).

B. Linear Ramp Initiation

$$\eta_S(0,t) = \eta_{S0}'t, \quad t > 0$$

$$= 0, \quad t \leq 0. \quad (4.15)$$

The appropriate boundary conditions become

$$\eta_S(\rho,0) = \eta_{S0}'\rho e^{-Gc\rho/2n}, \quad \rho > 0$$

$$= 0, \quad \rho \leq 0. \quad (4.16)$$

Substitution of (4.16) in (3.17) results in the equation

$$\frac{\eta_S}{\eta_{L0}} = \frac{2R^2y}{1+2R^2(e^y-y-1)}, \quad y > 0 \quad (4.17)$$

where

$$R^2 = (n\eta_{S0}'/Gc\eta_{L0})e^{Gt} \quad (4.18)$$

and y has the value defined in (4.8). In (4.18) and in the further examples below the parameter R represents approximately the peak photon density in units of η_{L0} , when $R \gg 1$. It follows that the peak photon density grows exponentially with gain constant $G/2 \text{ cm}^{-1}$. For $R \gg 1$, the calculations show that the total number of

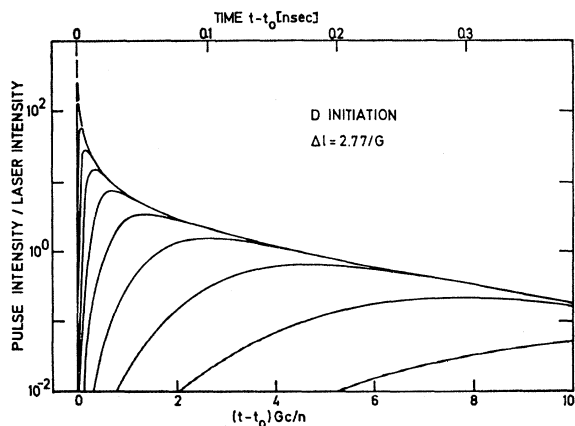


FIG. 4. Calculated normalized Raman pulse intensity as a function of time t for initial condition D (cubic).

photons can be written as

$$n_S = (4/\sigma) \ln(1.35R) \quad (4.19)$$

and the pulse duration is

$$\delta = 4\sqrt{3}/RG. \quad (4.20)$$

The time dependence of the pulse (4.17) is shown in Fig. 3 for the same equally spaced intervals as in Fig. 2. The factor-of-2 decrease in the gain constant for the peak intensity can be seen clearly.

C. Quadratic Initiation

$$\eta_S(0,t) = \eta_{S0}''t^2, \quad t > 0 \quad (4.21)$$

$$\frac{\eta_S}{\eta_{L0}} = \frac{3R^3y^2}{4+6R^3(e^y-\frac{1}{2}y^2-y-1)}, \quad y > 0 \quad (4.22)$$

where

$$R^3 = \frac{16 \eta_{S0}'' n^2 e^{Gt}}{3 G^2 c^2 \eta_{L0}}. \quad (4.23)$$

For $R \gg 1$ we obtain

$$n_S = (6/\sigma) \ln(1.12R) \quad (4.24)$$

and

$$\delta = 10/RG. \quad (4.25)$$

D. Cubic Initiation

$$\eta_S(0,t) = \eta_{S0}'''t^3, \quad t > 0 \quad (4.26)$$

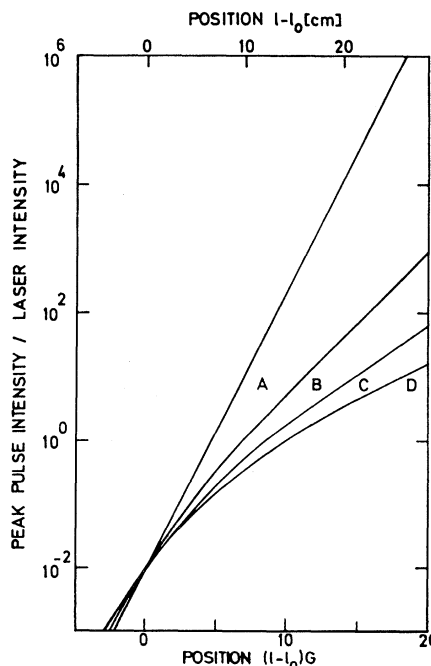


FIG. 5. Normalized peak Raman pulse intensity as a function of position $l-l_0$ for initial conditions A to D. l_0 is the reference length defined in Sec. IV. G was taken to be 0.7 cm^{-1} .

$$\frac{\eta_S}{\eta_{L0}} = \frac{4R^4 y^3}{27 + 24R^4(e^y - \frac{1}{6}y^3 - \frac{1}{2}y^2 - y - 1)}, \quad (4.27)$$

where

$$R^4 = 54\eta_{S0}''' n^3 e^{Gt} / \eta_{L0} G^3 c^3. \quad (4.28)$$

For $R \gg 1$ we obtain

$$n_S = (8/\sigma) \ln(0.98R) \quad (4.29)$$

and

$$\delta = 12.75/RG. \quad (4.30)$$

The time dependence of the D pulses is shown in Fig. 4 for the same intervals of l as in Figs. 2 and 3.

The behavior of the peak pulse intensity as a function of cell length is summarized in Fig. 5 for the various initiation conditions. For all the initiation conditions a reference length l_0 has been arbitrarily chosen as the length for which $\eta_S(\max)/\eta_{L0}$ is 10^{-2} . At l_0 the pulse duration and the pulse energy are also approximately independent of the initiation conditions. Figure 5 shows for all initial pulse shapes the exponential dependence of peak intensity on cell length l for $\eta_S(\max) \gg \eta_{L0}$. The lengths required for gain e are $1/G, 2/G, 3/G, 4/G$ for initial pulse shapes $A, B, C,$ and D . Physically the decrease in gain from $A \rightarrow D$ results from the increasingly gradual application of the Stokes pulse; in the limit of an infinitely slowly applied pulse, $\eta_S(\max)$ will in fact never exceed η_{L0} . For $\eta_S < 10^{-2}\eta_{L0}$, i.e., in the region $l < l_0$, the peak pulse height grows approximately as e^{Gt} for all initial pulse shapes.

The total pulse energy n_S is plotted in Fig. 6, in units of $1/\sigma$. Comparison of the energy dependence on cell length l relative to the $\eta_S/\eta_{L0} = 10^{-2}$ length shows only negligible dependence on the initiation condition.

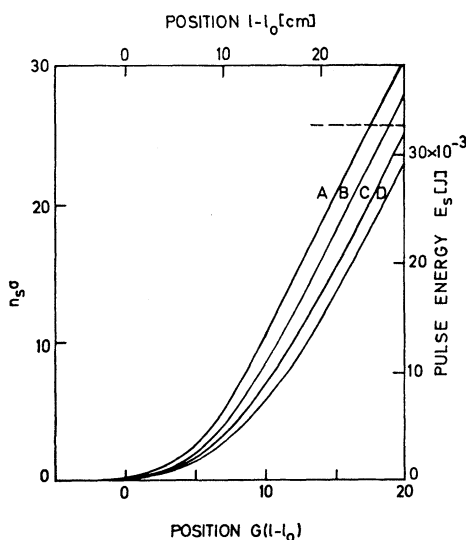


FIG. 6. n_S , total number of pulse photons cm^{-2} in units of $1/\sigma$ (or pulse energy E_S in joules), as a function of position $l-l_0$ for initial conditions A to D . The broken line indicates the pulse energy measured in our experiments.

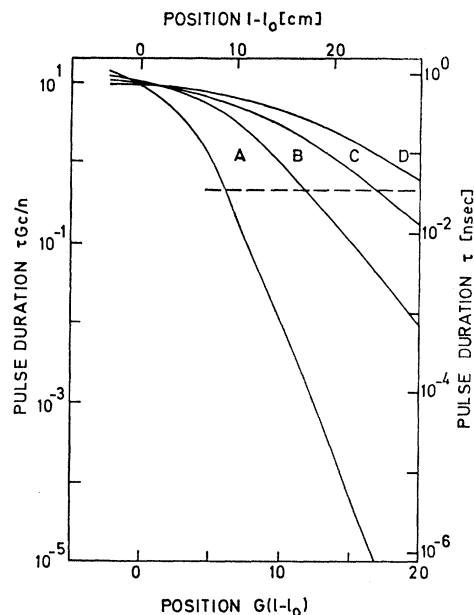


FIG. 7. Raman pulse duration τ as a function of position $l-l_0$ for initial conditions A to D . The broken line indicates the pulse duration measured in our experiments.

The typical decrease of pulse duration (in units of Gc/n) with increasing length is shown in Fig. 7 for the various initial conditions.

In the following part we consider a variety of initial conditions whose common feature is an exponential rise of the Raman light. This rapid rise can be justified from a physical model of the initial Raman pulse and will be discussed in detail in Sec. VIII. In E , the initiating pulse rises exponentially and then saturates. In F , a pulse width of finite duration rising and decaying exponentially (with different time constants) will be discussed (see insert of Fig. 8).

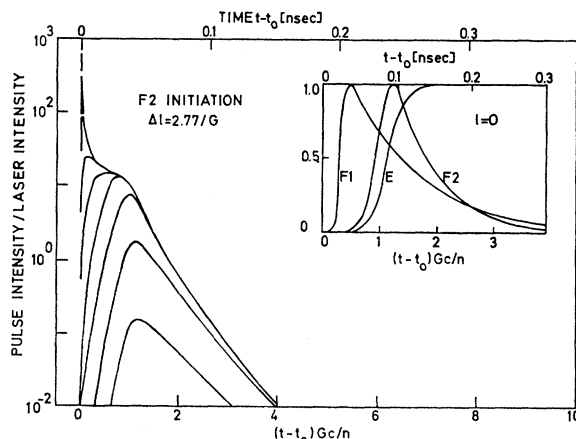


FIG. 8. Calculated normalized Raman pulse intensity as a function of time t for initial condition $F2$. The insert shows the normalized initial conditions E and F as a function of time t at the exit window of the cell $l=0$.

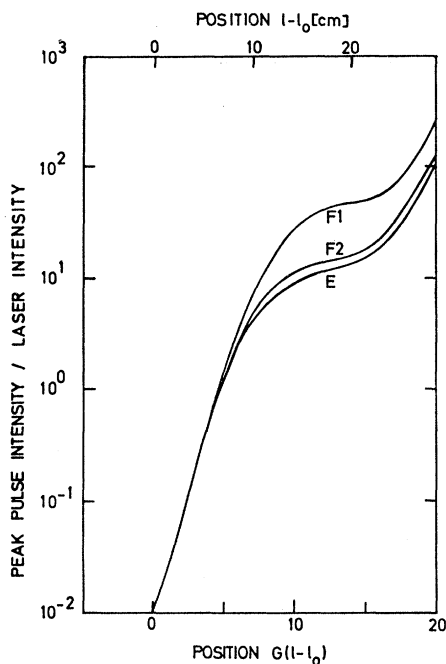


FIG. 9. Normalized peak Raman pulse intensity as a function of position $l-l_0$ for initial conditions E and F . l_0 is the reference length defined in Sec. IV. G was taken to be 0.7 cm^{-1} .

E. Exponential Initiation Followed by Saturation

$$\eta_s(0,t) = a \frac{e^{t/\tau_1} - 1}{e^{t/\tau_1} + b}, \quad t > 0 \tag{4.31}$$

$$= 0, \quad t \leq 0.$$

For $t \ll \tau_1 \ln b$, $\eta_s(0,t)$ rises exponentially with a rise time τ_1 . For $t \gg \tau_1 \ln b$ saturation takes place and η_s approaches a constant value a .

Using Eqs. (3.14), (3.17), and (4.1) we have calculated in Appendix A the peak pulse intensity, the pulse duration, and the pulse energy as a function of cell length for the initial condition (4.31). The following numbers were used: The time constant of the exponential rise was $\tau_1 = 10^{-11}$ sec, the ratio of the saturation value to the laser intensity was $a/\eta_{L0} = 10^{-4}$, and the constant b determining the duration of the exponential rise was 5×10^3 . The result of the calculations is shown in Figs. 9-11 and will be discussed at the end of this section.

F. Pulse Initiation with Exponential Rise and Decay

$$\eta_s(0,t) = a \frac{e^{t/\tau_1} - 1}{e^{t/\tau_2} + b} e^{(Gc/2n)t}, \quad t > 0 \tag{4.32}$$

$$= 0, \quad t \leq 0.$$

The main features of this initial condition are the exponential rise [$\eta_s \approx (a/b)(e^{t/\tau_1} - 1)$] for small t and the

exponential decay for large t (if $1/\tau_2 > 1/\tau_1 + Gc/2n$). The solution of the rate equations for this initiating pulse is given in Appendix A.

A very rough approximation to the solution has been obtained for $G(l-l_0) > 17$. In this case the photon number and length of the Raman pulse are given by

$$n_s \approx (4/\sigma) \ln(10R), \tag{4.33}$$

$$\delta \approx 10/RG. \tag{4.34}$$

We have treated two special cases, F_1 and F_2 with rise times $\tau_1 = 3 \times 10^{-12}$ sec and $\tau_1 = 10^{-11}$ sec, respectively. For both cases the ratio of the initial peak intensity of the pulse to the laser intensity was chosen to be $\eta_s^{\text{max}}/\eta_{L0} = 10^{-4}$ (cf. initial condition E). This number determines the ratio a/η_{L0} . The time constant τ_2 (which determines the decay of the pulse) was selected in such a way to give both initial pulses F_1 and F_2 a time duration of approximately 8×10^{-11} sec (length in air, 2.4 cm). The numbers used for the calculation were F_1 : $\tau_1 = 3 \times 10^{-12}$ sec and $\tau_2 = (20/21)\tau_1$. The results for different values of $b = 5 \times 10^3, 10^4, \text{ and } 5 \times 10^4$ showed only small differences in the range of experimental interest ($Gl < 20$). F_2 : $\tau_1 = 10^{-11}$ sec and $\tau_2 = \frac{4}{3}\tau_1$. Two curves for $b = 5 \times 10^3$ and 2×10^4 were calculated. The results of the calculations are shown in Figs. 8-11.

For the pulses E, F_1 , and F_2 (see insert Fig. 8) the ratio of peak pulse intensity/laser intensity, the pulse duration, and the total energy of the pulse are shown as a function of the distance $G(l-l_0)$ in Figs. 9-11. Figure 8 shows the growth of the input pulse F_2 and the change in shape in more detail. It is interesting to see in Fig.

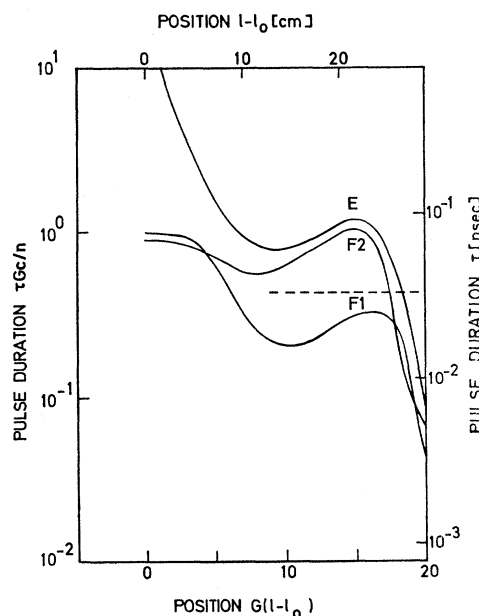


FIG. 10. Raman pulse duration τ as a function of position $l-l_0$ for initial conditions E and F . The broken line indicates the pulse duration measured in our experiments.

10 that the pulse duration (width at half-maximum intensity) first decreases, then increases slightly before decreasing quite strongly. The reason for this effect is seen quite readily in Fig. 8. First the peak of the pulse is more strongly amplified than the tail resulting in a shortening of the pulse; then the leading exponential edge begins to steepen rapidly, broadening the total pulse for some time, till finally a sharp peak develops at the beginning of the pulse. There is a considerable difference between Figs. 7 and 10; the pulses for the initial conditions *A* to *D* decrease continuously with pulse duration.

V. STEADY-STATE PULSE

The rate-equation analysis of Secs. III and IV shows that when the backward Raman pulse intensity exceeds the pump intensity its subsequent growth is linear in energy and exponential in peak intensity, irrespective of the initiation conditions. We show in this section that in the presence of small but finite attenuation the pulse is expected to approach a limiting steady-state condition with well-defined energy and duration, and having a characteristic intensity distribution. This pulse is similar to the limiting pulses expected in laser amplification.³⁴ When the pulse duration becomes so short as to be comparable with the damping time Γ^{-1} for the molecular vibrations, the rate-equation approximation (2.16) breaks down and a more complete analysis based on Eqs. (2.12)–(2.15) is necessary.

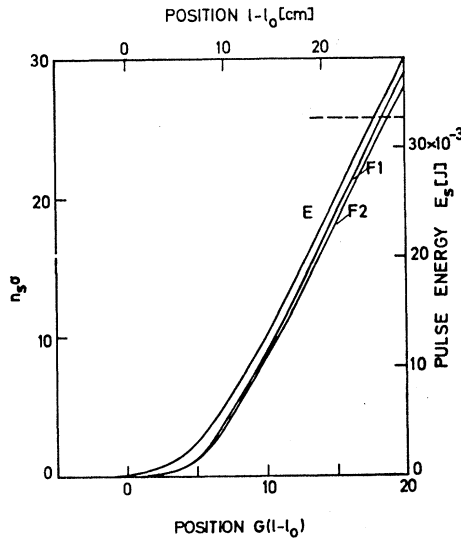


FIG. 11. Total number of pulse photons $\text{cm}^{-2} n_s$ in units of $1/\sigma$ (or pulse energy E_s) as a function of position $l-l_0$ for initial conditions *E* and *F*. The broken line indicates the pulse energy measured in our experiments.

³⁴ J. P. Wittke and P. J. Warter, *J. Appl. Phys.* **35**, 1668 (1964); C. L. Tang and B. D. Silverman, in *Physics of Quantum Electronics*, edited by P. L. Kelley, B. Lax, and P. E. Tannenwald (McGraw-Hill Book Co., New York, 1966), p. 280; F. T. Arecchi and R. Bonifacio, *IEEE J. Quantum Electron.* **QE1**, 169 (1965); J. A. Armstrong and E. Courtens, *ibid.* **QE4**, 411 (1968).

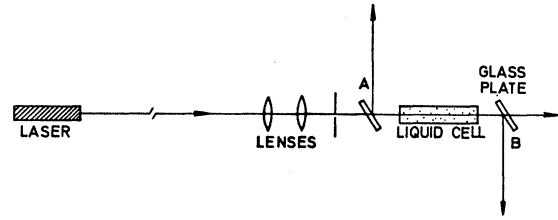


FIG. 12. Experimental arrangement for the investigation of stimulated Raman scattering.

Consider a Stokes pulse propagating in the $+z$ direction in a medium with attenuation constant γ_s . The $-z$ pump beam is assumed to have constant field E_{L0} at the pulse leading edge. Under steady-state conditions, $\partial E_s/\partial \rho = \partial E_L/\partial \rho = 0$, i.e.,

$$\frac{\partial E_s}{\partial z} + \frac{n_s}{c} \frac{\partial E_s}{\partial t} = 0, \quad (5.1)$$

$$\frac{\partial E_L}{\partial z} + \frac{n_s}{c} \frac{\partial E_L}{\partial t} = 0. \quad (5.2)$$

We combine Eqs. (5.1) and (5.2) with (2.12) to (2.15) to obtain the position-independent equations (5.3)–(5.6):

$$E_s = \frac{-2\pi N \omega_s}{n_s c \gamma_s} \frac{\partial \alpha}{\partial q} E_L q, \quad (5.3)$$

$$\frac{\partial E_L}{\partial t} = \frac{\pi N \omega_L}{2n n_L} \frac{\partial \alpha}{\partial q} E_s q, \quad (5.4)$$

$$\frac{\partial \Delta}{\partial t} = \frac{1}{2\hbar} \frac{\partial \alpha}{\partial q} E_L E_s q, \quad (5.5)$$

$$\frac{\partial q}{\partial t} + \frac{1}{2} \Gamma q = -\frac{1}{4m\omega_0} \frac{\partial \alpha}{\partial q} E_L E_s \Delta, \quad (5.6)$$

where n_s and n_L denote refractive indices at ω_s and ω_L , and $n \equiv \frac{1}{2}(n_s + n_L)$. The small pump attenuation γ_L does not play an important role and has been neglected. By elimination of E_s from (5.3)–(5.5) and from (2.17) we obtain

$$\frac{\partial \Delta}{\partial t} = \frac{4n}{cN} \frac{\partial N_L}{\partial t} \quad (5.7)$$

and

$$\Delta = (4n/cN)(N_L + N_0), \quad (5.8)$$

where N_0 is a constant. Also

$$N_s = -\frac{2n}{c\gamma_s} \frac{\partial N_L}{\partial t}. \quad (5.9)$$

The coupled equations for N_L and q^2 become

$$\partial N_L / \partial t = -u N_L q^2, \quad (5.10)$$

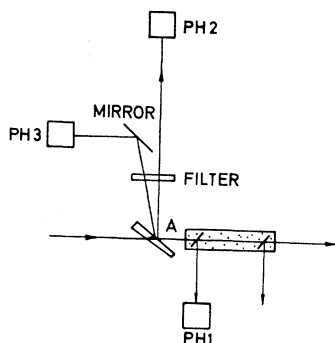


FIG. 13. Experimental arrangement for the determination of the total backward Raman energy as a function of position in the liquid cell.

$$\partial q^2 / \partial t + \Gamma q^2 = v N_L q^2 (N_L + N_0), \quad (5.11)$$

where

$$u = \frac{2\pi^2 N^2 \omega_S \omega_L}{n n_S n_L c \gamma_S} \left(\frac{\partial \alpha}{\partial q} \right)^2$$

and

$$v = \frac{32\pi^2 n \hbar \omega_S \omega_L}{m \omega_0 n_S n_L c^3 \gamma_S} \left(\frac{\partial \alpha}{\partial q} \right)^2.$$

For the experiments described in the present paper, the ratio of pump photon density to molecular density $n_L N_L / c N$ is 10^{-6} ; for this case Δ does not change significantly from its initial value. Equation (5.11) becomes

$$\partial q^2 / \partial t + \Gamma q^2 = v N_0 q^2 N_L \quad (5.12)$$

in the approximation that Δ is fixed.

An analytical solution of Eqs. (5.10) and (5.12) exists in the limit that $\Gamma \rightarrow 0$. As boundary conditions we take $N_L = N_{L0}$ and $q^2 = q_0^2$ at $t = t_0$, with $q_0^2 \ll v N_0 N_{L0} / u$. From (5.9), (5.10), and (5.12)

$$\frac{N_S}{N_{L0}} = 1.76 \frac{n \tau_S}{n_S \tau_L} \operatorname{sech}^2 \left(\frac{1.76t}{\tau_L} \right). \quad (5.13)$$

In (5.13) the time scale has been shifted to locate the maximum of the sech^2 function at $t=0$. We have introduced into Eq. (5.13) the damping time for the Stokes light due to linear losses $\tau_S = n_S (\gamma_{Sc})^{-1}$ and the width of the steady-state pulse at half-intensity:

$$\tau_L = 3.52 (\gamma_S / G'), \quad (5.14)$$

with $G' = G\Gamma$. G is the gain per cm of stimulated Raman scattering.

The intensity distribution of (5.13) has the same form as found for the limiting steady-state pulse in a laser amplifier³⁴ and in an absorbing medium under "stimulated transparency" conditions.³⁵ It will be shown in Sec. VIII that for the conditions in our experiments the measured Raman spike is far from the steady-state pulse described here.

³⁵ S. L. McCall and E. L. Hahn, Phys. Rev. Letters 18, 908 (1967).

The steady-state Raman pulse of Eq. (5.13) has the following interpretation. As the backward-traveling pulse is amplified and narrowed to a point where its duration τ becomes shorter than Γ^{-1} , the inverse linewidth of the gain curve, its spectral width becomes correspondingly broader with respect to Γ . The ratio of the pulse spectral width to the Raman linewidth is $\sim (\Gamma\tau)^{-1}$, and the effective gain seen by the pulse will be reduced from G by just this ratio, since only a fraction $\sim (\Gamma\tau)$ can effectively interact with the Raman line. A steady-state condition is reached when the effective gain $G(\Gamma\tau)$ is reduced to a value equal to the linear loss γ_S ; this condition determines the steady state pulse duration τ_L of (5.14). We note that the steady state pulse leaves the pump beam completely depleted.

VI. EXPERIMENTAL

A giant-pulse ruby laser, Q-switched by a solution of cryptocyanine in methanol, was used in our experiments. The laser beam showed an angular divergence of 10^{-3} rad and a frequency width smaller than 0.01 cm^{-1} ; the maximum output power was approximately 1 MW and the pulse duration was 15 nsec between half-maximum power points. Near the exit mirror the intensity distribution of the output beam measured over the cross section was nearly Gaussian with a width at half-intensity of 2 mm. Fabry-Perot measurements and the investigation of the laser pulse with a fast photoelectric detection system (over-all time constant ap-

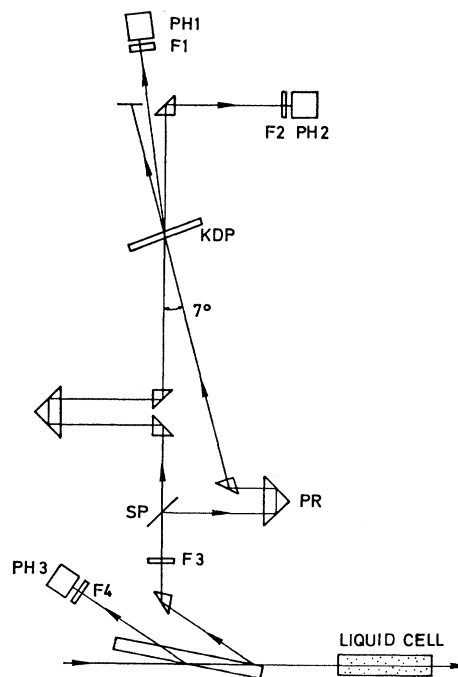


FIG. 14. Apparatus for the measurement of the autocorrelation function of the backward Raman pulse using the generation of second harmonic light in a KDP crystal. F1, 2, 3, 4 filters; PH photodiode; PR movable prism; SP beam splitter.

proximately 0.3 nsec) gave no evidence for a multi-frequency output. The laser intensity was increased by a factor of 9 by using an inverted telescope in front of the liquid cell (Fig. 12). A pinhole of approximately 0.6 mm diam reduced the diameter of the beam before entering the cell. The peak intensity of the laser pulse entering the liquid was 400 MW/cm². It should be noted that the distance between the laser and the liquid cell was kept large (4.2 m) to reduce the effects of reflected and reamplified Brillouin light. All measurements reported here were performed with CS₂ at room temperature.

In this paper we report (1) various properties of the forward- and backward-emitted Raman-Stokes light as well as the time dependence of the transmitted laser light, (2) the energy of the backward-traveling Raman-Stokes light as a function of position along the length of the cell, (3) the duration of the Raman light burst leaving the cell in the backward direction, (4) the time sequence and the peak powers of the forward- and backward-emitted Raman pulses.

(1) In Fig. 12 our experimental setup is shown schematically. Two glass plates were used to couple out some of the backward-emitted Raman and Brillouin light (A) and some of the transmitted laser light and forward-emitted Raman-Stokes light (B). The light beams at A and B were analyzed with Fabry-Perot interferometers, with a 3-prism glass spectrograph (resolution 1 Å) or with a fast photoelectric detection system consisting of photocells and fast oscilloscopes having an over-all rise time of approximately 0.3 nsec. In addition, near-field photographs of the cell windows were made using microscopes of different magnification placed in the beams A and B.

(2) The development of the backward-traveling Raman light pulse was investigated by measuring the total energy of the light pulse as a function of the position along the cell (see Fig. 13). Thin glass plates were immersed into the liquid and a small amount of Raman light was coupled out at various positions within the liquid cell. Measurements were made with a calibrated integrating photocell PH1. In addition the light pulse at the Raman-Stokes frequency leaving the entrance

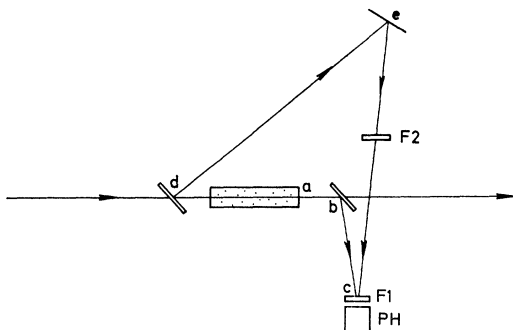


FIG. 15. Experimental arrangement for the simultaneous measurement of the backward and forward Raman emission. F1, 2 filters; PH photocell.

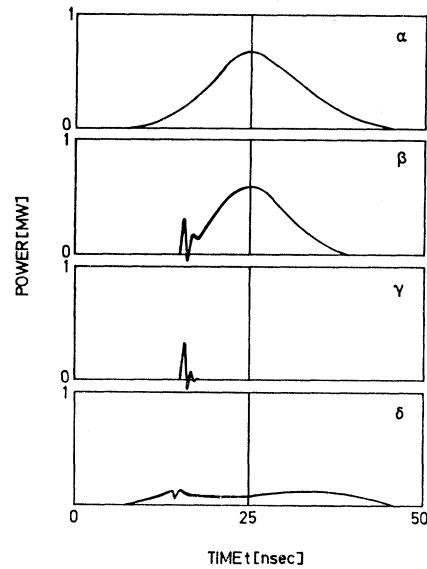


FIG. 16. Oscilloscope traces of the incident laser pulse (α), the total stimulated emission in the backward direction (β), the backward stimulated Raman emission alone (γ), and the transmitted laser light (δ).

window (A) was monitored by a fast photocell PH3 and an integrating photocell PH2 using appropriate filters.

(3) Figure 14 shows schematically the intensity autocorrelation technique^{20,36} which was used to measure the time duration of the Raman-Stokes spike. The backward-emitted Raman-Stokes light (monitored by the fast photocell PH3) was divided into two beams by a beam splitter SP. Both beams traversed a crystal of KDP for the production of second harmonic light. The direct generation of second harmonic light was investigated by a sensitive photomultiplier PH2. The coincidence photomultiplier PH1 placed between the two light beams measured the harmonic component having a propagation vector $\mathbf{k}_1 + \mathbf{k}_2$, providing a signal $J(\tau)$ proportional to $\int I_1(t)I_2(t+\tau)dt$. Here τ is the time delay between the two light pulses and I_1 and I_2 are their intensities. This time delay was varied during the experiment by changing the path difference by means of a movable prism PR. In order to obtain large second harmonic and coincidence signals the light beams with propagation vectors k_1 and k_2 were within several degrees of the phase matching angle.

(4) Figure 15 depicts schematically the experimental arrangement used to compare quantitatively the forward- and backward-emitted Raman-Stokes light. The forward-emitted Stokes pulse was measured directly at the exit window of the cell while the backward-emitted pulse was delayed by a known optical path. The latter signal reached the same photocell PH after being at-

³⁶ J. A. Armstrong, Appl. Phys. Letters **10**, 16 (1967); W. H. Glenn and M. J. Brienza, *ibid.* **10**, 221 (1967); H. P. Weber, J. Appl. Phys. **38**, 2231 (1967).

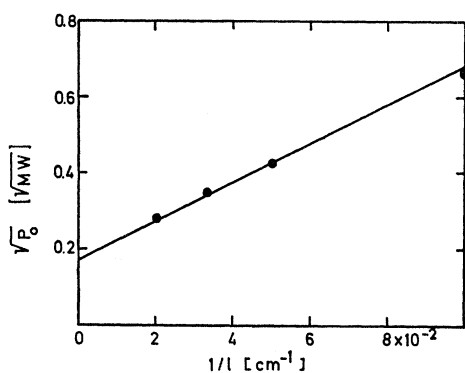


FIG. 17. Square root of the threshold power, $\sqrt{P_0}$, for self-focusing in CS_2 as a function of the reciprocal cell length $1/l$.

tenuated by filter F2. From the geometrical path difference and the observed time delay between the corresponding two pulses on the oscilloscope information as to the position of origin of the Raman pulses was obtained.

VII. EXPERIMENTAL RESULTS

A. Backward-Emitted Raman Pulse

In Fig. 16 the oscilloscope traces of the incident laser pulse (α), the total backward-emitted light consisting of Raman-Stokes light plus Brillouin-Stokes light (β), the Raman-Stokes light only (γ), and the transmitted laser pulse (δ) are depicted. The following points should be noted: The Raman-Stokes emission (β and γ) occurs several nanoseconds after the beginning of the laser pulse in the form of a sharp light burst shorter than 0.3 nsec, the time constant of the detection system. For CS_2 the Raman spike showed a frequency shift of 656 cm^{-1} , which is typical for the spontaneous Raman frequency of the most intense line of this material. Of special interest is the observation that the instantaneous Raman power exceeds the instantaneous laser power by an apparent factor of 2 or 3. This factor, being certainly a lower limit to the true value, will be discussed in greater detail below. Following the Raman-Stokes spike, intense Brillouin emission is observed [Fig. 16 (β)] with a characteristic Stokes shift of 0.193 cm^{-1} . The power conversion into Brillouin light showed a high efficiency of up to 90%. A detailed account of the generation of this Brillouin emission has been presented elsewhere.³⁷

Near-field photographs of the entrance window of the cell clearly indicated that the Raman-Stokes light is emitted over a broad area of 0.25 mm^2 which was of the same size as the area of the incident laser beam. The photographs showed in addition several Stokes filaments of diameters between 5 and 10μ . The area of these filaments was smaller by a factor of 10^3 than the total area of the Raman-Stokes emission; the intensity of these filaments exceeded the broad area emission by a

³⁷ M. Maier, Phys. Rev. **166**, 113 (1968).

factor less than 100. We have, therefore, neglected the emission in filaments in the following discussion.

The frequency spectrum of the backward Raman emission was investigated with a three-prism spectrograph. Four Stokes lines having a frequency separation of 656 cm^{-1} were observed on high-exposure photographs. It should be emphasized that the frequency spectrum of the backward and the forward emission (coming from one filament) showed sharp Raman lines without observable intensity between the laser and Stokes components.³⁸ The energies of the lines were measured simultaneously by the use of several photocells. The ratio of the energies of the first to the second to the third Stokes component was approximately 1:0.1:0.01. It is justified, therefore, to neglect higher Stokes components in the calculations below. The laser power transmitted by the liquid cell [Fig. 16 (δ)] showed the following behavior: After an initial rise, identical with that of the incident laser pulse [Fig. 16 (α)], a sharp break occurred at a definite power level P_0 . It could be shown that the magnitude of P_0 was a function of the length l of the liquid cell. It is interesting to note that the appearance of the Raman spike coincides in time with the break in the transmitted light power. During the rest of the pulse the transmitted laser power stayed somewhat below the level of P_0 . The small transmitted laser power results from the high Brillouin conversion³⁷ occurring for most of the laser pulse. It is the strong Brillouin scattering which prevents the recurrence of additional Raman spikes (see Sec. VIII).

In Fig. 17, $\sqrt{P_0}$ is plotted as a function of $1/l$, the reciprocal of the cell length. The observed proportionality strongly suggests that P_0 represents the threshold power for the self-focusing of the laser beam in the liquid. In addition, the value of P_0 extrapolated for

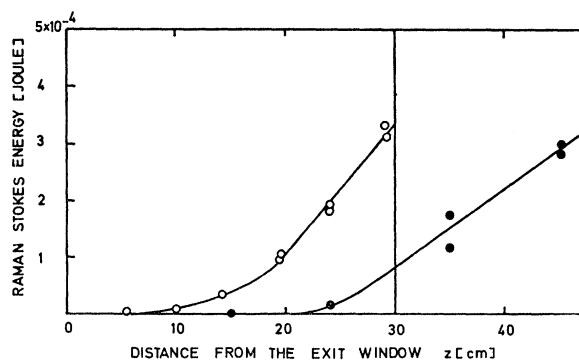


FIG. 18. Measured backward Raman-pulse energy as a function of the distance from the exit window of the liquid cell z . (O) cell length $l = 30 \text{ cm}$, (●) $l = 48.3 \text{ cm}$.

³⁸ Under focused and multimode conditions, broad-frequency spectra have been reported by R. G. Brewer, Phys. Rev. Letters **19**, 8 (1967); H. P. H. Grieneisen and C. A. Sacchi, Bull. Am. Phys. Soc. **12**, 686 (1967); Y. Ueda and K. Shimoda, Japan J. Appl. Phys. **6**, 628 (1967); F. Shimizu, Phys. Rev. Letters **19**, 1097 (1967); A. C. Cheung, D. M. Rank, R. Y. Chiao, and C. H. Townes, *ibid.* **20**, 787 (1968).

infinite cell length is found to be approximately 28 kW, in fair agreement with the critical power for self-focusing in CS₂.^{39,40} From these observations we wish to conclude that the backward-traveling Raman spike is initiated by the self-focusing action of the laser beam at the end of the cell. It should be mentioned that Fig. 17 is very similar to results obtained previously by a rather different method. Wang⁴⁰ has made time-integrated measurements of the stimulated Raman signal occurring in the forward direction and determined the threshold for self-focusing by the onset of stimulated Raman action. In our case, time-resolved measurements of the transmitted laser light have led us to the determination of the threshold power for self-focusing of the laser beam.

Additional evidence that self-focusing of the laser beam initiates the backward-traveling Raman-Stokes spike was obtained by photographing the exit window of the cell. It was found that a Raman-Stokes spike at the entrance window (A) was only present when self-trapping was seen at the exit window (B). In our experiments we observed consistently one Raman spike and one filament of approximately 5 μ in diameter.

B. Growth of the Raman Pulse

The total energy of the backward-traveling Raman-Stokes pulse is plotted in Fig. 18 as a function of distance z measured from the exit window. It is clearly seen from the graph that the measured energy values rise linearly with z after approximately half of the cell length. It was shown in Sec. IV that for all the initiation models considered, the Raman-Stokes energy is expected to be proportional to z . The slopes of the straight lines determined from Fig. 18 are $(2.3 \pm 0.4) \times 10^{-5}$ and $(1.4 \pm 0.4) \times 10^{-5}$ J/cm for cell lengths of 30 and 48.3 cm, respectively. These numbers will be shown to be in good

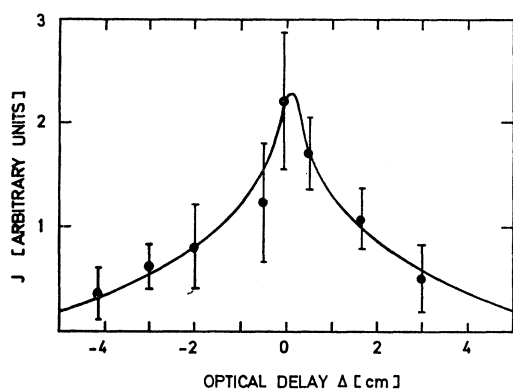


FIG. 19. Normalized output J of the coincidence photomultiplier proportional to the autocorrelation function $\int I_1(t)I_2(t+\Delta/c)dt$ versus optical delay Δ . The bars give the rms deviations from the average values.

³⁹ E. Garmire, R. Y. Chiao, and C. H. Townes, Phys. Rev. Letters **16**, 347 (1966).

⁴⁰ C. C. Wang and G. W. Racette, Appl. Phys. Letters **8**, 256 (1966).

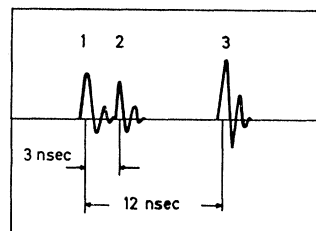


FIG. 20. Oscilloscope trace of the forward (1) and backward (3) Raman emission. The backward Raman light (3) has been attenuated by filters and delayed by 12 nsec compared to the forward pulse (1). Pulse (2) is a reflection of the backward Raman pulse from the entrance window of the liquid cell.

agreement with values calculated from the theory (see Sec. VIII).

At first glance it appears surprising that the Raman spike generated in the 48.3-cm cell does not contain substantially more photons than the spike produced in the 30-cm cell. The explanation for this observation rests in the initiation mechanism for the Raman spike. In the longer cell the self-focusing of the laser beam starts at a lower level (see Fig. 17) than in the shorter cell and—as a result—the backward-traveling Raman-Stokes light sees a lower laser power for its amplification.

C. Duration of the Raman Spike

In Fig. 19 the normalized output

$$J = \text{const} \times \int I_1(t)I_2(t+\tau)dt / \int I_1^2(t)dt$$

of the coincidence photomultiplier is plotted as a function of the path difference Δ between the two light pulses. The measured points represent average values of approximately five laser shots. The rms deviations are indicated. At half-maximum power points the path difference $\Delta_{1/2}$ is found to be approximately 2 cm. Computer calculations show that the pulse length is approximately $\frac{1}{2}\Delta_{1/2}$ for all initial conditions used. Experimentally we find a pulse length (in air) for our Raman spike of 1 cm corresponding to a pulse duration of 30 psec.

It is interesting to compare the length of the Raman spike with the coherence length of the Raman emission, determined from the frequency width of the first Stokes component. The observed first Stokes-Fabry-Perot rings have a frequency half-width of approximately 0.3 cm^{-1} . Assuming a signal with an abrupt increase and an exponential decay in time we calculate a coherence length of approximately 0.8 cm, which is in good agreement with the length of the spike estimated above. It appears, therefore, that the short pulse length of the Raman spike of only 1 cm is the major cause for the broadened Fabry-Perot pattern.

D. Forward and Backward Raman Emission

In Fig. 20 an oscilloscope trace representing three short light pulses is depicted. This picture was obtained

with the experimental system discussed in connection with Fig. 15. At the Raman-Stokes frequency we see three short signals labeled with the numbers 1, 2, 3. It was found that spike 1 and 2 were emitted through the exit window while spike 3 results from the backward emission leaving the cell through the entrance window. The distance between spikes 1 and 2 corresponds to twice the time necessary for the light to travel through the cell of 30 cm in length. The calculated time delay of $2 \times 30 \times 1.63/3 \times 10^{10} = 3.2$ nsec agrees well with the experimental value of 2.9 nsec. The power ratio of spike 2 to 3 was found to be 1:25 which strongly suggests that spike 2 is generated by reflection ($R \approx 4\%$) of the backward-traveling spike 3 at the entrance window. This assumption was substantiated by the following observation: When a pinhole was placed at the exit window of the cell and the cell inclined to such an extent that no reflected light could pass through the pinhole the second spike disappeared completely.

The 350-cm difference of the optical paths, (*adec*) - (*abc*), gives an expected time delay of 11.7 nsec (see Fig. 15). The measured time difference between spike 1 and 3 was 12.0 nsec. This value agrees well with the calculated number. We conclude from this result that the forward- and backward-emitted Raman spikes originate close to the exit window of the liquid cell (experimental accuracy 7 cm). This observation supports once more the finding discussed above that self-focusing close to the exit window initiates the backward-traveling Raman-Stokes spike.

With the fast photocell we have measured the apparent Raman-Stokes power P_S emitted in the forward and backward direction. It turned out that P_S (forward) varied around 10 kW by a factor of 2 while P_S (backward), which was more reproducible, had measured power values between 200 and 400 kW. These numbers for P_S are lower limits of the true peak power of the Raman spike. It has been shown above that the Raman spike has a duration of 30 psec, while the time constant of the measuring circuit was approximately 300 psec. The true peak power of the Raman spike will be discussed in the next section.

It should be repeated in this connection that the Raman emission in the forward direction is produced in a single small filament while the backward Raman light is emitted over a relatively broad area of approximately 0.25 mm².

VIII. DISCUSSION

Before analyzing our experimental observations, several remarks should be made on the theoretical gain factor, competing nonlinear processes, and on assumptions made in the theory of Secs. II to IV.

A. Theoretical Gain Factor for Stimulated Raman Scattering

It has been shown in the preceding theoretical studies that the gain factor g (or $G = gI_L$) enters the derived

equations quite critically. When various literature data are used for the evaluation of g a substantial spread in numbers is obtained. The different values are summarized here and discussed more fully in Appendix B. The gain factor can be written in the form [Eq. (B6) of Appendix B]

$$g = \frac{8\pi c^2 N}{\hbar \omega_S^3 n^2 \Delta \bar{\nu}} \frac{d\sigma'}{d\Omega}. \quad (\text{B6})$$

The Raman linewidth $\Delta \bar{\nu}$ of CS₂ is quite narrow, with previous investigations frequently hampered by instrumental resolution. We have adopted here the most recent result of Clements and Stoicheff,²³ who report $\Delta \bar{\nu} = 0.50 \pm 0.02$ cm⁻¹. The value of $d\sigma'/d\Omega$, the scattering cross section per solid angle, is not known with high accuracy. Quantitative measurements of $d\sigma'/d\Omega$ are difficult to perform because absolute values of the spontaneous scattering power of the Raman line are required. There are four independent sets of experiments which provide us with values for g :

First, the magnitude of $d\sigma'/d\Omega$ has been determined directly from the absolute scattering power at 656 cm⁻¹. A pulsed ruby laser ($\lambda = 6943$ Å) was used in this experiment.⁴¹ The data presented in Ref. 41 are believed to be accurate within a factor of 3. After taking into account the various Raman lines in the neighborhood of the 656-cm⁻¹ line we calculate a gain factor of $g = 7.5 \times 10^{-2}$ cm/MW (see Appendix B).

Second, the peak scattering cross section at the center of the Raman line has been measured with a cw argon laser at $\lambda = 4880$ Å. From these data⁴² we calculate $g = 1.2 \times 10^{-2}$ cm/MW (see Appendix B).

Third, the absolute scattering power of CS₂ is calculated from literature data of the relative scattering power of CS₂ to other liquids, such as toluene or benzene. For these liquids absolute scattering cross sections have been reported. In this way we obtain g values ranging from 1 to 3×10^{-2} cm/MW (see Appendix B).

Fourth, recently detailed investigations of the stimulated Raman scattering in CS₂ were made using subnanosecond laser pulses.⁴³ Good agreement with theory was obtained with a gain factor of $g = 1 \times 10^{-2}$ cm/MW.

In summary, we conclude that the data existing at the present time suggest a gain factor for CS₂ between 1 and 2×10^{-2} cm/MW. It will be shown below that our measurements on the backward-amplified Raman spike are consistent with a gain factor of $g = 1 \times 10^{-2}$ cm/MW, in good agreement with the forementioned value.

B. Competing Processes

It has been shown in Sec. VII that the light emission in the backward direction consists of the sharp and

⁴¹ G. Bret and G. Mayer, in *Physics of Quantum Electronics*, edited by P. Kelley, B. Lax, and P. Tannenwald (McGraw-Hill Book Co., New York, 1966).

⁴² J. G. Skinner and W. G. Nilsen, *J. Opt. Soc. Am.* **58**, 113 (1968).

⁴³ D. von der Linde, M. Maier, and W. Kaiser, *Phys. Rev.* (to be published).

intense Raman spike followed by stimulated Brillouin scattering. Stimulated Brillouin and Raman scattering are two competing processes with the steady-state gain factor for the Brillouin scattering ($g_B = 14 \times 10^{-2}$ cm/MW) being considerably larger than the gain factor for Raman scattering ($g_R = 1 \times 10^{-2}$ cm/MW). The observation that the Raman spike precedes the Brillouin emission is readily explained by the long acoustic phonon lifetime in CS_2 of 2.5 nsec. A time of this magnitude is required for g_B to grow to the full steady-state value.^{44,45} This fact explains why stimulated Raman emission occurs before stimulated Brillouin scattering has fully developed. Stimulated Raman scattering remains suppressed, however, for the rest of the pulse while strong Brillouin reflection ($\approx 90\%$) is generated within several millimeters from the entrance window of the liquid cell.³⁷ In this way laser light does not penetrate the liquid cell far enough to produce self-focusing and thereby to provide enough gain for the observation of further stimulated Raman emission. In fact, we have no evidence for a repetition of Raman emission in the forward or backward direction.

C. Rate-Equation Approximation

Before a quantitative comparison between the experimental and the theoretical results is made, an important assumption of the theory should be checked. In deriving the rate equations we have assumed [Eq. (2.16)] a large damping constant Γ for the molecular vibrations, i.e., $\partial q/\partial t \ll \frac{1}{2}\Gamma q$ or $2(\Delta q/q)(1/\Delta t) \ll \Gamma$. This condition is fulfilled since $\Delta q/q$ is certainly smaller than 0.1; we obtain $2 \times 0.1 \times (30 \times 10^{-12})^{-1} = 6 \times 10^9 \ll 2\pi \times 0.50 \times 3 \times 10^{10} = 9 \times 10^{10}$.

It should be pointed out that the backward-amplified Raman pulse reaches a pulse length of approximately 1 cm during the last several centimeters of its path. At this point we are approaching the limit of validity of our theoretical calculations: The frequency width of our Raman spike of 0.3 cm^{-1} is comparable with the width of the spontaneous Raman line $\Delta\bar{\nu} = 0.5 \text{ cm}^{-1}$.

D. Steady-State Pulse

In Sec. V we have derived an expression for the limiting duration τ_L of a steady-state pulse [Eq. (5.14)]. With a linear absorption of $\gamma_s \approx 10^{-3} \text{ cm}^{-1}$, $\Gamma = 10^{11} \text{ sec}^{-1}$, $g = 10^{-2} \text{ cm/MW}$, and $I_L = 72 \text{ MW/cm}^2$ one calculates a value $\tau_L = 5 \times 10^{-14} \text{ sec}$, far less than the value $3 \times 10^{-11} \text{ sec}$ observed in our experiments. We note, however, that the observed backward second Stokes signal (Sec. VII) represents an additional (nonlinear) absorption equivalent to an effective $\gamma_s \approx 1 - 10 \text{ cm}^{-1}$ in the region of the entrance window where the second Stokes intensity is $\sim 0.1 I_s$. This fact suggests that the limiting duration of the backward Raman pulse may not be

⁴⁴ N. M. Kroll, J. Appl. Phys. **36**, 34 (1965).

⁴⁵ D. Pohl, M. Maier, and W. Kaiser, Phys. Rev. Letters **20**, 366 (1968).

much shorter than 10^{-11} sec for the experimental arrangement described in this paper. Suppression of second Stokes generation should make possible the attainment of significantly shorter backward stimulated Raman pulses.

E. Initiation Mechanism of the Raman Spike

The investigation of the initiation mechanism of the backward Raman spike has indicated that self-focusing of the laser light close to the exit window of the cell plays a dominant role. We have further shown that a Raman filament occurs having a diameter of approximately 5μ and a duration shorter than $3 \times 10^{-10} \text{ sec}$.

As shown experimentally and in Secs. III and IV the strong amplification of the backward-traveling light pulse exhausts the laser pump light. Calculations using Eq. (3.18) show that the laser is substantially weakened within a time of approximately $5 \times 10^{-10} \text{ sec}$. This effect may contribute to the short duration of the laser filament and of the forward-emitted Raman-Stokes light.

It should be noted that we have clearly separated the forward Raman emission from other spurious effects. In most of the previous investigations reflections of the backward spike from the cell window and from the laser mirrors were not distinguished from the forward emission (and were measured together with it). The fluctuations which we observed in the power output of the forward- and backward-emitted Raman light are believed to be due to changes in the properties of the laser emission which strongly influence the self-focusing action.

F. Initial Conditions of the Calculations

The calculation of the time behavior of the Raman spike (Sec. IV) indicated that the output pulse development depends on the initial conditions. In order to illustrate in a general way the process of pulse formation, steepening, and sharpening we have treated the simplified initial conditions A to D (step function, linear ramp, etc.).

As discussed in the preceding chapter the backward Raman pulse is initiated by self-focusing of the laser light close to the exit window of the cell. Since the lifetime of the filaments is approximately 10^{-10} sec initial conditions with a finite pulse duration appear to be more appropriate for our problem. If the initial conditions A to D are cut off after approximately 10^{-10} sec the calculations of the output Raman pulses (Figs. 5 to 7) are still valid for large values of the cell length l [$G(l-l_0) > 15$]. For small lengths l , differences between both types of initial conditions are found, which are of no significance for our experimental situation.

In Figs. 9 to 11, calculations for two exponentially rising pulses of short duration (F_1 and F_2 in the insert of Fig. 8) are presented. We feel that these pulses represent more realistic initial conditions for our problem than conditions A to D. The time dependence of the pulses F_1

TABLE I. Experimental gain factor g for stimulated Raman scattering and ratio of the peak Raman intensity to the laser intensity $(\eta_S/\eta_{L0})_{\max} \simeq R$ for different initial conditions.

Initial condition	g (10^{-3} cm/MW)	R
<i>A</i>	2.3	19.4
<i>B</i>	5.6	27.6
<i>C</i>	8	27.9
<i>D</i>	10	27.8
<i>E, F</i>	8	19

and F_2 was chosen on the following grounds: (1) The formation of the filaments occurs extremely rapidly with the time constant of the Kerr effect (approximately 2×10^{-12} sec in CS_2). (2) There is a nonstationary build-up of the Raman light having a time constant in the order of the lifetime of the molecular vibration (10^{-11} sec in CS_2). (3) The filament starts at the exit window of the cell and increases in length with a velocity v which is determined by the rise time of the giant pulse (in the nanosecond range).

Considering these three points in more detail we conclude that an exponentially rising pulse of finite length describes the time dependence of the initial Raman light rather well. The rise time of the exponential function was estimated to be around 10^{-11} sec or smaller. For initial condition *F* we have treated two cases, $\tau_1 = 3 \times 10^{-12}$ sec and $\tau_1 = 10^{-11}$ sec. The pulse duration was taken to be 8×10^{-11} sec, which is approximately the duration of the filament.

Initial condition *E* describes a pulse with exponential rise followed by saturation; the results for this pulse demonstrate that the finite pulse duration of the initial pulse has little influence on the output pulse for long cell lengths.

G. Estimate of the Reference Length l_0

For a convenient comparison of the results of the different initial conditions (*A* to *F*) a reference length l_0 was chosen at which the ratio of the maximum Raman intensity to the laser intensity reaches 10^{-2} . The value of l_0 can be estimated in the following two ways.

First, we assume that the power emitted in the Raman filament in the forward and backward direction is approximately the same ($\simeq 10$ kW). If we consider the solid angle subtended by the laser light and the solid angle into which the backward Raman light is emitted, we estimate a ratio of the maximum initial Raman intensity to laser intensity of 10^{-5} to 10^{-4} . With these values reference lengths l_0 between 3 and 10 cm are obtained (for a cell length of 30 cm), depending on the initial condition (*A* to *F*). The method of calculation can be easily seen for initial condition *A* using Eq. (4.8a).

Second, the axial intersection l_A of the linear part of the energy dependence on position z can be used to estimate the reference length l_0 . From the experimental results (Fig. 18) we obtain directly l_A (measured) ≈ 15 cm (for cell length 30 cm). From the theoretical calcula-

tions (Figs. 6 and 11) we get the difference between the axial intersection and the reference length, l_A (calculated) $- l_0$, which varies between 6 and 12 cm, depending on the initial conditions. (It should be noted that the difference $l_A - l_0$ is independent of the gain factor g .) Since l_A (measured) should be equal to l_A (calculated) we obtain l_0 values between 3 and 9 cm in agreement with the first estimate.

H. Experimental Determination of the Gain Factor g

There are two independent experimental results, the energy E_S and the duration δ of the backward-emitted Raman pulse, which can be used to determine an experimental gain factor g . The expressions for the pulse duration δ [Eqs. (4.13), (4.20), (4.25), (4.30), and (4.34)] and the pulse energy E_S [Eqs. (4.10), (4.19), (4.24), (4.29), and (4.33)] contain two unknown quantities, the gain factor g and the ratio of maximum Stokes intensity to laser intensity $\eta_{S\max}/\eta_{L0} \simeq R$. Using the measured quantities $E_S = 3.3 \times 10^{-4}$ J, $\delta(\text{air}) = 1$ cm, and $I_L = 72$ MW/cm² we have calculated g and R for the various initial conditions. The results of these calculations are summarized in Table I. The similarity of the g and R values for a variety of initial conditions is noteworthy. For the following comparison between theory and experiments we use $g = 10^{-2}$ cm/MW, which lies within the range of accuracy both of the experimental and theoretical results.

I. Energy of the Raman Spike

In Sec. VII results are presented for the total backward Raman energy as a function of position z in the liquid cell (Fig. 18). The initial region, where the energy rises nonlinearly, is not discussed here because of inadequate experimental accuracy for the small energy values.

In the linear region the experimentally determined slope can be compared with the theoretical slope S [calculated from Eq. (4.14)]. The theoretical slope is the same for all initial conditions and is independent of the gain factor; it represents simply the sweeping out of the incoming pump beam. S is given by $2(n\omega_S/c\omega_L)P_L$. During the passage of the Raman pulse through the liquid cell (1.6 nsec) the laser power increases slightly. For the calculation of S we have used average values of 180 and 130 kW for the cell lengths 30 and 48.3 cm, respectively. The results are $S_{\text{meas}}(30 \text{ cm}) = (2.3 \pm 0.4) \times 10^{-5}$ J/cm and $S_{\text{calc}}(30 \text{ cm}) = 1.9 \times 10^{-5}$ J/cm, $S_{\text{meas}}(48.3 \text{ cm}) = (1.4 \pm 0.4) \times 10^{-5}$ J/cm, and $S_{\text{calc}}(48.3 \text{ cm}) = 1.3 \times 10^{-5}$ J/cm. There is good agreement between the measured and calculated values.

The Raman energy measured at the end of the cell (length 30 cm) was $E_S = 3.3 \times 10^{-4}$ J ($\pm 20\%$). According to Figs. 6 and 11 this amount of energy is acquired within a distance $l - l_0$, depending upon the initial conditions (see Table II). For the initial pulses F_1 and F_2 one finds $l - l_0 \approx 26.0$ cm, which suggests a reference

TABLE II. Distances $l-l_0$, obtained from the measured pulse energy and duration, and corresponding ratio of peak Raman intensity to laser intensity $(\eta_S/\eta_{L0})_{\max}$. For further discussion see text.

Initial condition	Energy $n_s\sigma=25.8$		Pulse duration $\tau Gc/n=0.45$	
	$l-l_0(\text{cm})$	$(\eta_S/\eta_{L0})_{\max}$	$l-l_0(\text{cm})$	$(\eta_S/\eta_{L0})_{\max}$
<i>A</i>	24.3	4×10^6	8.3	4
<i>B</i>	26.4	500	16.7	15
<i>C</i>	28.2	66	23.6	22
<i>D</i>	29.6	24	36.0	26
<i>E</i>	25.6	36.5		
<i>F1</i>	26.3	106		
<i>F2</i>	26.8	67		

length l_0 of several centimeters in good agreement with estimates presented above.

J. Duration of the Raman Spike

The length of the backward Raman spike was determined to be approximately 1 cm in air (Fig. 19). This experimental result will be first compared with the theoretical results for the initial conditions *A* to *D*. According to the theoretical calculations (Fig. 7) a pulse length of 1 cm (in air) will be reached when the pulse has traversed a certain distance $l-l_0$ depending on the initial condition. The distances $l-l_0$ are also listed in Table II. It should be noted that only initial conditions *C* and *D* give results which are consistent with a cell length of 30 cm.

Next we consider the theoretical results for initial conditions *E*, and *F1*, *F2* (see Fig. 10). As discussed in Sec. IV, the pulse duration τ calculated for *E* and *F* is quite different from that of *A* to *D*. Up to distances $l-l_0$ of 23 cm τ does not change substantially, having values within the experimental accuracy of the measured number of 1 cm (broken line in Fig. 10). For a cell length of 30 cm and a reference length of 5 cm the expected pulse lengths are between 0.7 and 1.5 cm (see Fig. 10), in good agreement with the measured value of 1 cm.

K. Peak Power of the Raman Spike

The ratio of the Raman peak intensity to the laser intensity, $\eta_{S\max}/\eta_{L0} \approx R$, has been estimated in Sec. VIII H; consistently, values between 20 and 30 were calculated for several initial conditions (see Table I).

We have also estimated the same ratio from Figs. 5 and 9 using values of $l-l_0$ obtained from the energy data in Sec. VIII I and from the pulse duration in Sec. VIII J. The numbers determined in this way are listed in the third and fifth column of Table II. Peak intensity ratios between 20 and 100 are found. The completely

unreasonable values obtained for the initial conditions *A* and *B* are not surprising, since the step function and the linear ramp are physically unrealistic initial conditions. We consider the latter determination of the peak power less accurate because small uncertainties in $l-l_0$ give rise to large errors in R . Combining all our information a value for the peak power ratio between 20 and 30 is suggested.

IX. SUMMARY

It has been shown in the preceding sections that a considerable amount of experimental data is consistent with a model in which a backward-traveling Raman pulse interacts strongly with the incoming laser pulse. There is strong evidence that the initiating Raman pulse is generated in a filament at the end of the liquid cell. During its path the Raman pulse is amplified to intensities exceeding those of the incident laser light. A pulse length of 1 cm was measured in our experimental system.

ACKNOWLEDGMENTS

We are highly indebted to M. Stanka (Technische Hochschule Munich) for collecting much of the experimental data contained in this paper, and to Dr. S. L. Shapiro (BTL), who carried out several corroborative experiments. We also wish to thank K. Wecht (BTL) and W. Rother (Technische Hochschule Munich) for their help with the computer calculations.

APPENDIX A: SPECIAL SOLUTIONS OF THE RATE EQUATIONS FOR INITIAL CONDITIONS *E* AND *F*

1. Exponential Initiation Followed by Saturation (*E*)

$$\eta_S(0,t) = a \frac{e^{t/\tau_1} - 1}{e^{t/\tau_1} + b}, \quad t > 0$$

$$= 0, \quad t \leq 0. \quad (4.31)$$

Using Eqs. (3.14), (3.17), and (4.1) the development of the Raman pulse is calculated to be

$$\frac{\eta_S}{\eta_{L0}} = \frac{2R^2}{d} \frac{1 - e^{-dv}}{(b^{-1} + e^{-dv})[1 + 2R^2 F(y)/d]}, \quad (A1)$$

with

$$d = 2n/Gc\tau_1 \quad \text{and} \quad R^2 = (ad/2b\eta_{L0})e^{Gt}. \quad (A2)$$

The analytical solution (A1) is only valid if d is an integer. Since τ_1 is not known with high accuracy this restriction is not important. We have used the abbreviations

$$F(y) = 1 - e^y - e^y(1+b) \left\{ \frac{s}{db^{1/d}} \ln \frac{1+b^{1/d}e^{-y}}{1+b^{1/d}} - \frac{2}{db^{1/d}} \sum_{\nu=0}^{(d-s-2)/2} \left[P_\nu(y) \cos \frac{2\nu+1}{d}\pi - Q_\nu(y) \sin \frac{2\nu+1}{d}\pi \right] \right\}, \quad (A3)$$

with

$$P_\nu(y) = \frac{1}{2} \ln \frac{(b^2)^{1/d} e^{-2y} - 2b^{1/d} e^{-y} \cos[(2\nu+1)/d]\pi + 1}{(b^2)^{1/d} - 2b^{1/d} \cos[(2\nu+1)/d]\pi + 1} \tag{A4}$$

and

$$Q_\nu(y) = \arctan \frac{b^{1/d} e^{-y} - \cos[(2\nu+1)/d]\pi}{\sin[(2\nu+1)/d]\pi} - \arctan \frac{b^{1/d} - \cos[(2\nu+1)/d]\pi}{\sin[(2\nu+1)/d]\pi}. \tag{A5}$$

s is 0 or 1, depending on whether d is even or odd.

2. Pulse Initiation with Exponential Rise and Decay (F)

$$\eta_S(0,t) = a \frac{e^{t/\tau_1} - 1}{e^{t/\tau_2} + b} e^{(Gc/2n)t}, \quad t > 0$$

$$= 0, \quad t \leq 0. \tag{4.32}$$

The solution of the rate equations for this initiating pulse is

$$\frac{\eta_S}{\eta_{L0}} = \frac{2R^2}{d} \frac{e^y(e^{-fy} - e^{-fhy})}{(b^{-1} + e^{-fhy})[1 + 2R^2 \bar{F}(y)/d]}, \tag{A6}$$

$$\bar{F}(y) = \frac{e^y}{fh} \left\{ \ln \frac{1 + b e^{-fhy}}{1 + b} - \frac{b}{b^{1/h}} \left[s \ln \frac{1 + b^{1/h} e^{-fy}}{1 + b^{1/h}} - 2 \sum_{\nu=0}^{(h-s-2)/2} \left(\bar{P}_\nu(y) \cos \frac{2\nu+1}{h} \pi - \bar{Q}_\nu(y) \sin \frac{2\nu+1}{h} \pi \right) \right] \right\}, \tag{A7}$$

with

$$\bar{P}_\nu(y) = \frac{1}{2} \ln \frac{(b^2)^{1/h} e^{-2fy} - 2b^{1/h} e^{-fy} \cos[(2\nu+1)/h]\pi + 1}{(b^2)^{1/h} - 2b^{1/h} \cos[(2\nu+1)/h]\pi + 1} \tag{A8}$$

and

$$\bar{Q}_\nu(y) = \arctan \frac{b^{1/h} e^{-fy} - \cos[(2\nu+1)/h]\pi}{\sin[(2\nu+1)/h]\pi} - \arctan \frac{b^{1/h} - \cos[(2\nu+1)/h]\pi}{\sin[(2\nu+1)/h]\pi}. \tag{A9}$$

s is 0 or 1 depending on whether h is even or odd.

APPENDIX B: CALCULATION OF THE GAIN FACTOR g FOR STIMULATED RAMAN SCATTERING

In Sec. II we have derived the cross section σ for stimulated scattering [Eq. (2.21)]. σ is related to the gain factor g by

$$g = \sigma n / ch\omega_L. \tag{B1}$$

Using Eq. (2.21) we obtain for g

$$g = \frac{8\pi^2 \omega_S N}{n^2 c^2 m \Gamma \omega_0} \left(\frac{\partial \alpha}{\partial q} \right)^2. \tag{B2}$$

For the calculation of g we need the value of $\partial \alpha / \partial q$, which can be derived from the experimental spontaneous Raman scattering cross section $d\sigma' / d\Omega$. The relation between $d\sigma' / d\Omega$ and $\partial \alpha / \partial q$ is derived as follows: From ordinary scattering theory we obtain

$$d\sigma' / d\Omega = \omega_s^4 \alpha_{01}^2 / c^4, \tag{B3}$$

with

$$d = \frac{2n}{Gc\tau_1}, \quad f = \frac{2n}{Gc\tau_1(h-1)}, \quad \text{and} \quad R^2 = \frac{ad}{2b\eta_{L0}} e^{Gt}.$$

The time constant τ_2 which determines the exponential decrease of the initiating pulse has only little influence on the results. It was chosen arbitrarily to be $\tau_2 = \tau_1 \times (h-1)/h$ where h is an integer. The analytical solution is valid only if this condition is fulfilled. Again the following abbreviations have been used.

where α_{01} is the polarizability matrix element of the Raman transition. α_{01} is connected with $\partial \alpha / \partial q$ by the relation

$$\alpha_{01}^2 = (\partial \alpha / \partial q)^2 q^2. \tag{B4}$$

If we consider the energy of the harmonic oscillator to be the same in the classical and quantum-mechanical derivation, we obtain $q^2 = \hbar / 2m\omega_0$ and

$$d\sigma' / d\Omega = \omega_s^4 \alpha_{01}^2 / c^4 = \omega_s^4 (\partial \alpha / \partial q)^2 \hbar / 2m\omega_0 c^4. \tag{B5}$$

The gain factor can now be written

$$g = \frac{16\pi^2 c^2 N}{\hbar \omega_s^3 \Gamma n^2} \frac{d\sigma'}{d\Omega} = \frac{8\pi c N}{\hbar \omega_s^3 n^2 \Delta \bar{\nu}} \frac{d\sigma'}{d\Omega}, \tag{B6}$$

where $\Gamma = 2\pi c \Delta \bar{\nu}$, with $\Delta \bar{\nu}$ the full width at half-maximum intensity of the spontaneous Raman line.

For a Lorentzian shape of the Raman line the integrated scattering cross section $d\sigma' / d\Omega$ can be replaced by the peak cross section at the center of the line

$$\frac{d\sigma' p}{d\Omega} = \frac{2cd\sigma' / d\Omega}{\pi \Delta \nu}. \tag{B7}$$

For the calculation of the gain factor of CS₂ we have used the following values in Eq. (B6): $\Delta\bar{\nu}=0.5\text{ cm}^{-1}$, $N=10^{22}\text{ cm}^{-3}$, $n=1.61$, and $\omega_s=2.59\times 10^{15}\text{ sec}^{-1}$. All quantities are known for CS₂ with good accuracy except the spontaneous scattering cross section $d\sigma'/d\Omega$. There are three sources of information on this quantity.

First, $d\sigma'/d\Omega$ has been calculated from absolute power measurements of the spontaneous Raman line at 656 cm^{-1} using a ruby light source.⁴¹ The accuracy of these data for CS₂ is estimated to be a factor of 3.⁴⁶ Since the Raman intensity was integrated⁴⁶ over a frequency interval of approximately 100 cm^{-1} , $(d\sigma'/d\Omega)_{\text{measured}}$ contains contributions from all Raman lines around $656\pm 50\text{ cm}^{-1}$. From knowledge⁴⁷ of the relative integrated intensities of these lines we can estimate the true scattering cross section of the 656-cm^{-1} line. We arrive at $(d\sigma'/d\Omega)_{\text{CS}_2}=2.4\times 10^{-29}\text{ cm}^2$ and a value of $g=7.5\times 10^{-2}\text{ cm/MW}$.

Second, the peak scattering cross section $d\sigma_p'/d\Omega$ at the center of the Raman line has been reported very recently⁴² for various substances at $\lambda=4880\text{ \AA}$. While the accuracy of these measurements is quite high for most liquids (several percent) the situation is less favorable for CS₂ where the instrumental resolution is approximately equal to the width of the 656-cm^{-1} line. Using the value $d\sigma_p'/d\Omega=4.7\times 10^{-30}\text{ cm}^2$ (corrected for the ruby wavelength) we calculate from Eqs. (B6) and (B7) a gain factor $g=1.2\times 10^{-2}\text{ cm/MW}$.

Third, the scattering cross section for CS₂ is available from measurements of the absolute value of $d\sigma'/d\Omega$ of other liquids⁴⁸ (e.g., toluene and benzene) and from

⁴⁶ We are indebted to Dr. G. Mayer for a private communication on these subjects.

⁴⁷ H. W. Schrötter, *Z. Elektrochem.* **64**, 853 (1960).

⁴⁸ F. J. McClung and D. Weiner, *J. Opt. Soc. Am.* **54**, 641 (1964); T. C. Damen, R. C. C. Leite, and S. P. S. Porto, *Phys. Rev. Letters* **14**, 9 (1965).

the reported relative scattering power of these liquids and CS₂ compared to CCl₄.⁴⁹⁻⁵¹ Following Ref. 52 the ratio of the absolute scattering cross sections of two liquids can be written as

$$\frac{(d\sigma'/d\Omega)_1}{(d\sigma'/d\Omega)_2} = \frac{h_1\bar{\nu}_2(\bar{\nu}_L-\bar{\nu}_1)^4}{h_2\bar{\nu}_1(\bar{\nu}_L-\bar{\nu}_2)^4} \times \frac{1-\exp(-hc\bar{\nu}_2/kT)}{1-\exp(-hc\bar{\nu}_1/kT)} \\ \times \frac{(1+a_2)(n_1^2+2)^2n_1}{(1+a_1)(n_2^2+2)^2n_2} \times \frac{S_1}{S_2}.$$

1 stands for CS₂, 2 for the second liquid; $h_{1,2}$ is the degree of degeneracy of the Raman line, $\bar{\nu}_{1,2}$ the wave number of the Raman displacement, $\bar{\nu}_L$ the wave number of the light source, $a_{1,2}$ is the degree of depolarization of the Raman light for linearly polarized incoming light, $n_{1,2}$ the index of refraction, and S_1 and S_2 are the relative scattering powers with respect to CCl₄. Using the numbers for the relative scattering power S given in Refs. 49 to 51 and the numbers for $(d\sigma'/d\Omega)_{\text{toluene,benzene}}$ reported in Ref. 48, we calculate values for $(d\sigma'/d\Omega)_{\text{CS}_2}$ between 4 and $10\times 10^{-30}\text{ cm}^2$. The corresponding gain factors g are between 1 and $3\times 10^{-2}\text{ cm/MW}$.

⁴⁹ H. J. Bernstein and G. Allen, *J. Opt. Soc. Am.* **45**, 237 (1955); G. Allen and H. J. Bernstein, *Can. J. Chem.* **32**, 1124 (1954); J. P. Jesson and H. W. Thompson, *Proc. Roy. Soc. (London)* **A268**, 68 (1962).

⁵⁰ K. Venkatesvarla and G. Thyagarajan, *Z. Physik* **154**, 70 (1959); N. K. Sidorov, L. S. Stal'makhova, and L. I. Barmanova, *Opt. i Spektroskopiya* **13**, 783 (1962) [English transl.: *Opt. Spectry. (USSR)* **13**, 443 (1962)].

⁵¹ The relative scattering power S of CS₂ compared to CCl₄ has been measured by H. W. Schrötter with a He-Ne gas laser to be 1.87. We wish to thank Dr. Schrötter for making available his data prior to publication.

⁵² G. Eckhardt and W. G. Wagner, *J. Mol. Spectry.* **19**, 407 (1966).